Investigation on Giant Dielectric Constant Material

$CaCu_3Ti_4O_{12}$

高介電常數材料 $CaCu_3Ti_4O_{12}$ 的研究

YUAN, Wenxiang

苑文香

A Thesis Submitted in Partial Fulfillment
of the Requirements for the Degree of
Doctor of Philosophy
in
Physics

The Chinese University of Hong Kong
August 2010

ProQuest LLC
789 East Eisenhower Parkway
P.O. Box 1346
Ann Arbor, MI 48106-1346

Thesis/Assessment Committee

Professor KUI, Hin Wing (Chair)
Professor HARK, Sui Kong (Thesis Supervisor)
Professor NG, Hang Leung Dickon (Committee Member)
Professor MEI, Wai Ning (External Examiner)

Abstract

$CaCu_3Ti_4O_{12}$ (CCTO), an unusual perovskite-like material, is known for extraordinarily high (often reaching 10^4) and relatively frequency independent dielectric constant. Recently, it has drawn a lot of attention, because of its potential applications in microelectronics and microwave devices.

In this investigation, CCTO powders were synthesized by two routes, a conventional solid-state reaction and a wet-chemistry method. Three kinds of materials, polyvinyl alcohol (PVA, an organic binder), boric oxide (B_2O_3, a well-known glass former), hafnium oxide (HfO_2, a material with high dielectric constant ~25), were added to the pre-reacted CCTO powder and sintered into ceramics. The effects of these additives on the microstructures, or electric and dielectric properties of CCTO ceramics were investigated. In addition, CCTO thin films were also successfully prepared. The AC conductivity, impedance, and complex dielectric permittivity were used to analyze the data. These observations were well explained in terms of an internal barrier layer capacitor (IBLC) model with Maxwell-Wagner (MW) dielectric relaxation.

摘要

作為一種不尋常的鈣鈦礦型的材料，$CaCu_3Ti_4O_{12}$(CCTO)由於其擁有的非常高的介電常數具有相對的頻率不依賴性，因而有名。更因為其在超小型的和微波的器件上的應用潛力，所以廣受關注。

在這次的研究中，CCTO 粉末被用傳統的固態反應和濕化學這兩種方法合成。然後聚乙烯醇(polyvinyl alcohol,PVA,一種有機粘合劑)，氧化硼(boric oxide,B_2O_3,一種熟知的玻璃原料)，和氧化鉿(hafnium oxide,HfO_2,一種高介電(~25)的材料)三種不同性質的材料再加入到製備好的 CCTO 粉末中，通過燒結成陶瓷材料，以便研究這些添加物對 CCTO 陶瓷的形貌，電學或者介電性質的影響。同時，CCTO 薄膜也被成功的製備了。交流電導，複阻抗和複介電常數被用來分析測量到的資料。基於內部障礙層電容器(internal barrier layer capacitor,IBLC)的模型和相應的麥斯威爾-瓦格納(Maxwell-Wagner,MW)介電弛豫，所有觀察到的現象都得到了很好的解釋。

Acknowledgement

First of all, I would like to extend my sincere gratitude to my supervisor, Professor Sui-Kong Hark, who offered me this great opportunity and the support through the entire graduate school. During the course of my research, he demonstrated enormous patience, provided me with excellent guidance, not to mention tolerated many of my mistakes. All these impressed me tremendously and encouraged me to pursue my goal diligently. He is truly an excellent teacher and researcher.

In addition, I wish to thank Professor Wai-Ning Mei, who gave me many suggestions and contributed considerable amount of time and effort to improve my thesis.

I also want to thank Doctor Hai-Yang Xu, who assisted me during the investigation on the dielectric-property measurement and preparation of CCTO thin films.

Finally, I am indebted to my colleagues who helped me greatly during my research.

Contents

Chapter 1 Introduction

1.1 Background

The giant dielectric constant in calcium copper titanate, $CaCu_3Ti_4O_{12}$ (CCTO), has a high frequency dielectric constant of about 10^4-10^5, which is practically frequency independent between DC and 10^6 Hz and possesses good temperature stability over a range from 100 to 400 K [1-4]. This remarkable property makes it highly suitable for technological applications in capacitive memories and mobile phones [1,5]. Meanwhile, CCTO is also a Pb-free dielectric material, and will not be an environmental hazard.

In fact, CCTO was first synthesized in 1967, and its crystalline structure was found out in 1979 [6,7]. In 2000, Subramanian et al. [1] reported that it exhibits a high dielectric constant. Due to the high and stable dielectric constant, it has been the subject of extensive study in recent years. That is because, with the miniaturization of microelectronic devices, the demand of high dielectric constant materials is increasing rapidly. Dielectric materials can be applied to several devices, including dynamic random access memory (DRAM), ceramic capacitors, and microwave devices [8-11]. However, CCTO ceramics have high dielectric constant values from 10^3 to 10^6, depending on their fabrication process [12-15]. So the dielectric constant is very sensitive to the experimental conditions.

From the X-ray diffraction studies, the crystalline structure of CCTO is found to be the *Im3* space group [1,7], a perovskite-like constructed by superimposing a body centered ordering of Ca and Cu ions and a pronounced tilting of the titanium centered octahedra. The lattice parameter is deduced to be 7.391 Å, and the Ti cation is found

to reside at the octahedral coordination, with a heavily distorted Ti-O-Ti bond angle of 141°, which alters the coordination of Ca and Cu cations and leads to a square-planar environment for Cu and 12-coordinated icosahedron for Ca. That is to say, the Ca and Cu cations occupy crystallographically distinct *A* sites with a coordination of 12 and 4, respectively. The Cu-O distance shows no variation with temperature in the range of 50-300 K, due to the high rigidity of its bond [16]. Therefore, it is unlikely that the high dielectric-constant phenomenon is caused by a lattice structure change, and/or other related intrinsic mechanisms, such as ferroelectric phase transition. Hence, it is necessary to turn to the other direction, namely, searching for extrinsic mechanisms.

Considerable amount of efforts aimed at understanding the extrinsic origins have been put forward by many research groups: characterizations of the temperature and frequency dependences of the permittivity and impedance of CCTO and related compounds, such as $Bi_{2/3}Cu_3Ti_4O_{12}$ [17,18], $La_{2/3}Cu_3Ti_4O_{12}$ [18], and $SrCu_3Ti_4O_{12}$ [18], had been carried systematically, and it was found that, in all these compounds, a Debye-like relaxation with a dielectric constant independent of temperature and frequency was detected for a wide range. In complex impedance measurements, there are evidences of two dielectric responses with different intensities and frequencies were observed. These two dielectric responses were related to semiconducting grains and other insulating grain boundaries, and ascribed as the Maxwell-Wagner (MW) relaxation of the interfacial polarization, which was due to oxygen deficiency occurred at the regions between grains and grain boundaries and generated the detected Debye-like relaxation and large dielectric constant. Thus, a generally accepted scenario, the internal barrier layer capacitance (IBLC) model [4,19-23], is constructed to explain most of the dielectric behaviors of CCTO and related materials.

1.2 Empirical model and essential physical quantities

In this section, we shall introduce the equivalent circuit primarily used to analyze the experiment data of dielectric properties, the physical quantities, such as complex impedance Z^*, complex dielectric permittivity ε^*, AC conductivity σ_{AC}, and nonlinear coefficient α, and their relations with each other. All these quantities are useful in understanding the dielectric properties of CCTO samples.

1.2.1 Equivalent circuit

The resistor-capacitor equivalent circuit shown in Fig. 1.1 is inspired by the observation and study of the MW relaxation in the dielectric spectroscopy, and often used to analyze the dielectric responses of CCTO ceramic samples. Identification of the contributions from the bulk grain and grain boundary of the ceramic material is derived from fitting the experimental response to the equivalent circuit, usually comprised of a series of parallel resistor-capacitor (R-C) pairs. The circuit consists of a series array of two subcircuits, one of which represents grain and the other grain boundary effects. Each subcircuit is composed of a resistor and a capacitor joined in parallel. Let (R_g, R_{gb}) and (C_g, C_{gb}) be the resistances and capacitances of the grains and grain boundaries, respectively.

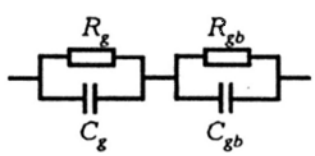

Fig. 1.1 Equivalent circuit used to represent the dielectrical properties of CCTO ceramics that exhibit grain (R_g, C_g) and grain boundary (R_{gb}, C_{gb}) effects.

1.2.2 Complex impedance (Z^*)

From the above mentioned equivalent circuit of IBLC model, the complex impedance (Z^*) can be shown to be:

$$Z^*(\omega) = (\frac{1}{R_g} + j\omega C_g)^{-1} + (\frac{1}{R_{gb}} + j\omega C_{gb})^{-1} = Z' - jZ'', \quad (1)$$

$$Z' = \frac{R_g}{1+(\omega R_g C_g)^2} + \frac{R_{gb}}{1+(\omega R_{gb} C_{gb})^2} \quad , \quad (2)$$

$$Z'' = R_g(\frac{\omega R_g C_g}{1+(\omega R_g C_g)^2}) + R_{gb}(\frac{\omega R_{gb} C_{gb}}{1+(\omega R_{gb} C_{gb})^2}) \quad , \quad (3)$$

where ω is the angular frequency, $j = \sqrt{-1}$, Z' and Z'' are the real and imaginary parts of Z^*. From Equation (1), it can be seen that when $\omega \to 0$, $Z^*(\omega) \to R_g + R_{gb}$. Specifically, in the case of CCTO ceramics, we have to assume $R_g << R_{gb}$ and $C_g << C_{gb}$ in order to deduce the intrinsic mechanism discussed later.

Graphically, the complex impedance of Equation (1) appears as two separate semicirclar arcs when $1/R_gC_g >> 1/R_{gb}C_{gb}$ in the Z' vs Z'' plot (complex impedance plot) as shown in Fig. 1.2. The larger arc is due to the grain boundary (large resistance) responses at low frequencies and the smaller arc is due to the bulk grain (small resistance) responses at high frequencies. At the maximum of each arc, $\omega_{max}\tau = 2\pi f_{max}\tau = 1$, where f is the frequency of the applied field, and $\tau (= R_xC_x,\ x=g$ *or gb*) is the relaxation time. When plotting the complex impedance, one may obtain both semicircles, when each term has distinctly different f_{max} values at different ranges of frequencies. In order to distinguish the components in the equivalent circuit (Fig. 1.1) in the complex impedance diagram, f_{max} must differ by at least two orders of magnitude. In actual measurements, it is hard sometimes to obtain both semicircular arcs in the *complex impedance* plot, especially for the small arc associated with the

interior of the bulk grain, because its f_{max} at room temperature is usually beyond the highest available frequency of impedance analyzers. So, the nonzero Z' intercept of the larger arc at high frequencies usually represents the resistance of grains (R_g). Each semicircle is separated into the two portions by $(2\pi f_{max} R_x C_x)_{Z'=Z'_{max}} = 1$, right one (lower frequencies) and the left one (higher frequencies). In most cases that will be presented later, we observed that the arcs corresponds to lower frequency (right) portion of the small semicircle, and the higher frequency (left) portion of the large semicircle, due to the limit of the measuring temperature and frequency.

From the above statements, we can see that each parallel *R*-*C* pair represents a component with different capacitance and resistance values. So in the experiments, we also find out the other components different from grains and grain boundaries, such as domain boundaries and sample surface layers, which will described in detail in Chapter 2. As a result, there will be four parallel *R*-*C* pairs in series in the equivalent circuit, so four semicircular arcs should be observed. In fact, because their f_{max} values are too close, their corresponding semicircular arcs are not separated out from each other in complex impedance spectrum. Therefore, we have to adopt another more efficient method to analyze the data, which will be introduced in Section 1.2.3.

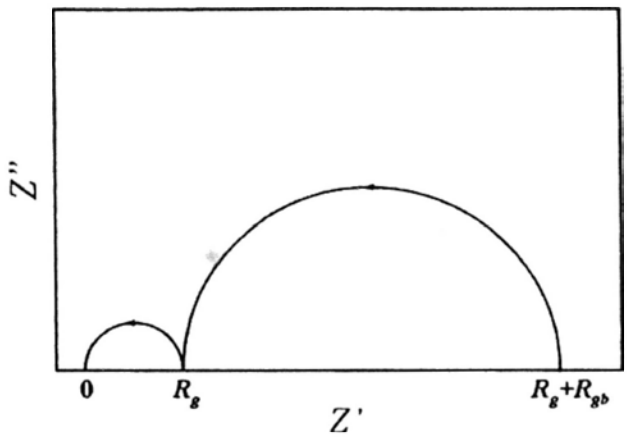

Fig. 1.2 Complex impedance spectrum corresponding to the IBLC model. Arrows indicate the direction of increasing frequency.

1.2.3 Complex dielectric permittivity (ε)*

Another presentation of the dielectric response, the complex dielectric permittivity (ε^*), can be calculated as following:

$$\varepsilon^* = \varepsilon' - j\varepsilon'' = \frac{1}{j\omega C_0 Z^*} \quad , \tag{4}$$

where C_0 is the empty cell capacitance, $j = \sqrt{-1}$, ε' and ε'' are the real and imaginary parts of ε^*.

In the Cole-Cole plot of complex dielectric permittivity (ε'' versus ε'), we usually notice arcs close in shape to semicircles in Chapter 2, which are associated with the different dielectric relaxation processes, that is to say, each semicircle corresponds to each parallel *R-C* pair. The complex dielectric permittivity diagram can sometimes reveal more information about the relaxation processes involved with grains and grain boundaries.

1.2.4 Effective dielectric constant (ε') and IBLC model

Following the thorough investigations of complex impedance and dielectric permittivity, the high dielectric constant of CCTO at radio frequencies is associated with the IBLC effect, arised from the core/shell structure. Accordingly, each grain contains a conductive "core" at the interior of the grain (bulk CCTO) and a uniform insulating shell on the outside. The insulating shell is formed by local reoxidation of ions, and called as the grain boundary [24], and its thickness is assumed to be independent of the grain size, since it is controlled by the rate of diffusion. Because of different electric properties between the bulk CCTO grain and grain boundary, that is $R_g << R_{gb}$ and $C_g << C_{gb}$, the "effective" dielectric constant (ε') of the core/shell structure at low frequencies can be approximated as:

$$\varepsilon' \sim \varepsilon_{gb}(t_g + t_{gb})/t_{gb}, \quad (5)$$

where ε_{gb} is the dielectric constant of the insulating grain boundary phase (but is often assumed to be the same as that of the bulk phase), t_g the average grain size and t_{gb} the average grain-boundary thickness [17,25,26]. Like many other research groups [26,27], we think the ε_{gb} value is approximately 100.

If $t_{gb} << t_g$, the effective dielectric constant can be further simplified as [28-32]:

$$\varepsilon' \sim \varepsilon_{gb}(t_g/t_{gb}). \quad (6)$$

Therefore, within the IBLC model, the dielectric constant is tightly related with the average size of grains and the thickness of grain boundaries; more specifically, the ratios of grain size versus grain-boundary thickness.

1.2.5 AC conductivity (σ_{AC})

To study the transport properties, we introduce the AC conductivity (σ_{AC}) that is

defined as:

$$\sigma_{AC} = \omega\varepsilon_0\varepsilon' tan\delta = \omega\varepsilon_0\varepsilon' D = \omega\varepsilon_0\varepsilon'', \quad (7)$$

where ε_0 is the permittivity in vacuum, $\omega = 2\pi f$ and f is the frequency, and $tan\delta\,(= D)$ is the dielectric loss.

Usually, σ_{AC} increases with the frequency. We note that the AC conductivities of CCTO ceramics fall within the range of those of the semiconductors. It is generally believed that the presence of shallow levels in the band structure of CCTO renders it semiconducting [33,34]. The shallow levels arise from the formation of oxygen vacancies, expressed as: O_o (oxygen ion at normal site) $\rightarrow$ V_o^{2+} (oxygen vacancy) + $2e^- + \frac{1}{2}O_2$, results in the high conductivity of CCTO. The frequency-dependent AC conductivity has been successfully utilized to distinguish the contributions of different insulating layers to dielectric response, such as sample surface, grain boundary, domain boundary, each of which acts as a depletion layer inducing its own respective dielectric relaxation. The details will be described in Chapter 2.

1.2.6 Nonlinear coefficient (α)

In the majority of situations, a polycrystalline material has a small leakage current passing through its microstructure, when it is subjected to a voltage below its characteristic breakdown voltage [35]. Only when the voltage exceeds the breakdown voltage, it becomes conductive and a sudden current increase is observed. In general, when the applied voltage returns to a value lower than the breakdown voltage, the material returns to its highly resistive state. In fact, there are two voltage ranges in the current voltage characteristics of the material below breakdown voltage: a very low

voltage range in which the current-voltage behavior is expected to be Ohmic; a relatively high voltage range in which the current-voltage behavior is highly non-Ohmic and nonlinear. The material possessing a significant nonlinear current–voltage (*I-V*) characteristic is called a varistor.

In the experiments reported here, we adopt a popular choice that sets the breakdown electric field (E_b) of CCTO as the applied electric field that induces 1 mA cm^{-2} current density [36,37]. Then the numerical value for the nonlinear coefficient α was obtained by fitting a linear regression of the log$J$ versus log$E$ plot from the current density-electric field (*J-E*) characteristic of the samples within the 0.1-1 mA cm^{-2} range.

Since the current-voltage characteristic of varistors is nonlinear, hence it is expressed as.

$$I = KV^{\alpha}, \quad \alpha = \frac{d(\log I)}{d(\log V)} = \frac{d(\log J)}{d(\log E)} \tag{8}$$

where K is a constant and α is the nonlinear coefficient.

1.3 Experimental methods

Usually, a CCTO powder is prepared in a process that involves solid-state reactions, which yields large crystal grains with a wide range of sizes. In order to produce a powder with small grains, another experimental method, a wet-chemistry method [38], is also selected, which is operated without using a glove-box or refluxing the solution, significantly reducing costs and time. In comparison, the solid state method is easier to operate, and provides ample amounts of powder; the wet chemistry method synthesizes less amount of powder at much lower temperature (800

°C) and in shorter time (1 h). Detailed descriptions of these two methods will be summarized in Sections 1.3.1 and 1.3.2.

The extraordinary high dielectric constant of CCTO renders it a potential candidate for DRAM capacitor material. Compared with bulk materials, the films are more suitable for their potential applications in microelectronics and micromechanics, especially thin films with thickness below 1 μm. In our research, the CCTO thin films were prepared by using radiofrequency (rf) magnetron sputtering method, the schematic of which is shown in Fig. 1.3, and the experimental details will be stated in Section 1.3.3.

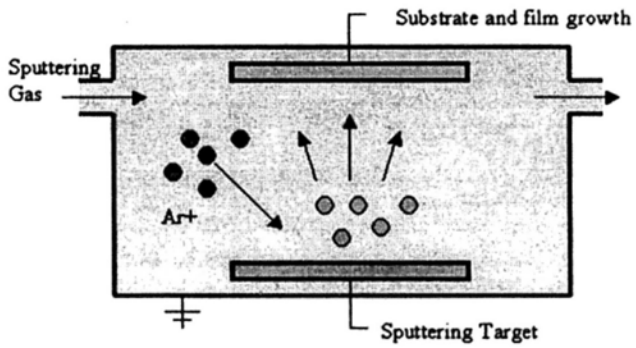

Fig. 1.3 Schematic image of rf magnetron sputtering.

1.3.1 Preparation of CCTO powder by a solid-state reaction

CCTO powder was synthesized by a traditional solid state method. Stoichiometric amounts of $CaCO_3$ (99.0%), CuO (99%), and TiO_2 (98%) starting powders were milled by a planetary mill machine for 2 h at a rotational speed of 240 rpm. Afterwards, the mixture was first calcined at 900 °C for 10 h, and then its temperature was quickly brought up to 1100 °C in for a short duration of 10 min. The ramping rate was 20 °C/min. Finally, the furnace was allowed to cool to room temperature by turning off its heating [39].

1.3.2 Preparation of CCTO powder by a wet-chemistry method

A wet-chemistry method was used to synthesize fine grain CCTO powder. $Ca(NO_3)_2 \cdot 4H_2O$ (99%), $Cu(NO_3)_2 \cdot 2.5H_2O$ (99.99%) and $Ti[OCH(CH_3)_2]_4$ (97%) were weighed accurately according to the stoichiometric ratio. 2.84 g $Ti[OCH(CH_3)_2]_4$ was first mixed with 1 g acetylacetone by magnetic stirring. 1.92 g citric acid previously dissolved in 3 ml de-ionized water was added to the titanium solution and stirred for 30 min. 0.59 g $Ca(NO_3)_2 \cdot 4H_2O$ and 1.74 g $Cu(NO_3)_2 \cdot 2.5H_2O$ were dissolved in 20 ml de-ionized water. They were added into the titanium-citric acid solution. After adding several drops of aqueous ammonia, the solution was heated to 70 °C to evaporate the water, resulting in a blue gel, which was dried at 450 °C for 15 min. The resultant porous powder was calcined at 800 °C for 1 h [40].

1.3.3 Preparation of CCTO thin film by rf magnetron sputtering method

A CCTO powder was prepared by the same solid state reaction described in Section 1.3.1. It was then pressed into a pellet of 6 cm diameter and 5 mm thick under a pressure of 16 MPa. Afterwards, the pellet was sintered at 1000 °C in air for 10 h and cooled to the room temperature. Thus the target used in the rf magnetron sputtering machine was ready. The films were sputtered on a $Pt/Ti/SiO_2/Si$ substrate whose distance from the CCTO target was 6 cm. The vacuum chamber was initially pumped down to a base pressure below 1×10^{-4} Pa, and the working pressure during sputtering was 1 Pa. The rf power was fixed at 150 W with a power density of 5.31 W/cm^2; the deposition time was 2 h. The chamber was back-filled with Ar and the substrate temperature was maintained at 480 °C during sputtering.

1.3.4 Characterization equipment

In this dissertation, we utilize the following equipment for different purposes. The crystalline phase of the sintered ceramic pellets was characterized by X-ray diffraction (XRD, Rigaku) using the Cu-Kα radiation produced at 40 kV and 160 mA. The microstructures of the ceramic pellets were investigated by scanning electron microscopy (SEM, LEO 1450 VP) with 20 kV as the typical accelerating voltage. Elemental analysis was carried out using the energy-dispersive X-ray (EDX) detector associated with SEM. For electrical measurements, the pellets were polished with SiC paper, and then silver paint was applied on both surfaces of the pellet. Dielectric measurements were performed at room temperature over a frequency range from 40 Hz to 30 MHz at an applied voltage of 1 V root mean square (RMS) amplitude at room temperature. In the frequency range of 40 Hz to 100 kHz, we used a NF Electronic Instruments Model 2330 *LCR* meter, and in the frequency rang of 75 kHz to 30 MHz, an Agilent 4285A Precision *LCR* meter.

1.4 Studies of CCTO ceramics with different additions and CCTO thin films

In Chapter 2, we describe the preparation and study of CCTO ceramics using the powder synthesized by the wet chemistry method sintered at 900 °C and 1050 °C for 3 h. Their microstructure evolutions and dielectric properties were studied. Through a careful investigation of their dielectric responses with the help of complex dielectric permittivity diagrams and frequency-dependent AC conductivity, we found out are three different extrinsic effects associated with the sample surface, grain boundary and domain boundary for their giant dielectric constants. Though the domains were

scarcely observed in the fine grains (<2 μm) [41,42], the dielectric relaxation corresponding to the domain boundaries was apparently observed in both the CCTO ceramics with comparatively finer and larger grains, which results in much larger dielectric constant. The results presented here are different from those of CCTO ceramics prepared by the solid state reaction.

On top of that, we also prepared three different series of CCTO ceramics with the addition of three different kinds of materials: polyvinyl alcohol (PVA), boric oxide (B_2O_3) and hafnium oxide (HfO_2). These series of samples were all fabricated by using the solid state reaction. The effects of the additives on the microstructures, dielectric and electric properties of CCTO ceramics are reported in Chapters 3, 4, and 5. We select the additives based on their special properties: namely, PVA is a well-known organic binder, and usually used in the sintering process to help the formation of compacted polycrystals [43-47]; B_2O_3 forms a glassy phase with a low melting point (450 °C) and it has a low viscosity at the sintering temperature [48]; HfO_2 is a high dielectric-constant material with $\varepsilon' = 22\text{-}25$ [49]. Due to their specific properties, after mixing with CCTO powder, we notice that these additives modify in different ways the grain size distribution, average grain size, and /or grain-boundary thickness of the ceramic samples. Hence, these CCTO+addition systems exhibit a variety of intriguing dielectric phenomena that are interesting to study.

Finally, CCTO thin films were synthesized by using rf magnetron sputtering, and their microstructures and dielectric properties were studies and described in Chapter 6. During an annealing process, it is well known that temperature is crucial to the microstructures and dielectric properties of films, we shall elaborate the details in Chapter 6.

References

[1] M.A. Subramanian, L. Dong, N. Duan, B.A. Reisner, A.W. Sleight, *High dielectric constant in $ACu_3Ti_4O_{12}$ and $ACu_3Ti_3FeO_{12}$ phase*, J. Solid State Chem. **151** (2000) 323-325.

[2] L. Fang, M. Shen, J. Yang, Z. Li, *The effect of SiO_2 barrier layer on the dielectric properties of $CaCu_3Ti_4O_{12}$ films*, J. Phys. D: Appl. Phys. **38** (2005) 4236–4240.

[3] C.C. Homes, , T. Vogt, , S.M. Shapiro, , S. Wakimoto, A.P. Ramirez, , *Optical response of high-dielectric-constant perovskite-related oxide*, Science **293** (2001) 673–676.

[4] T.B. Adams, D.C. Sinclair, A.R. West, *Giant barrier layer capacitance effects in $CaCu_3Ti_4O_{12}$ ceramics*, Adv. Mater. **14** (2002) 1321–1323.

[5] A.F.L. Almeida, P.B.A. Fechine, M.P.F. Graça, M.A. Valente, A.S.B. Sombra, *Structural and electrical study of $CaCu_3Ti_3FeO_{12}$ (CCTO) obtained in a new ceramic procedure*, J. Mater. Sci.: Mater. Electron. **20** (2009) 163-170.

[6] A. Deschanvres, B. Raveau, F. Tollemer, Bull. Soc. Chim. Fr. **11** (1967) 4077.

[7] B. Bochu, M.N. Deschizeaux, J.C. Joubert, *Synthèse et caractérisation d'une série de titanates pérowskites isotypes de $[CaCu_3](Mn_4)O_{12}$*, J. Solid State Chem 29 (1979) 291-298.

[8] E. Atanassova, A. Paskaleva, *Challenges of Ta_2O_5 as high-k dielectric for nanoscale DRAMs*, Microelectron. Reliab. 47 (2007) 913-923.

[9] S. Kwon, C.C. Huang, M.A. Subramanian, D.P. Cann, *Effects of cation stoichiometry on the dielectric properties of $CaCu_3Ti_4O_{12}$*, J. Alloys Compd. **473** (2009) 433-436.

[10] P.B.A. Fechine, A. Tavora, L.C. Kretly, A.F.L. Almeida, M.R.P. Santos, F.N.A. Freire, A.S.B. Sombra, *Microstrip antenna on a high dielectric constant substrate: $BaTiO_3$ (BTO)-$CaCu_3Ti_4O_{12}$ (CCTO) composite screen-printed thick films*, J. Electron. Mater. **35** (2006) 1848-1856.

[11] A.F.L. Almeida, P.B.A. Fechine, L.C. Kretly, A.S.B. Sombra, *$BaTiO_3$ (BTO)-$CaCu_3Ti_4O_{12}$ (CCTO) substrates for microwave devices and antennas*, J. Mater. Sci. **41** (2006) 4623-4631.

[12] M.J. Pan, B.A. Bender, *A bimodal grain size model for predicting the dielectric constant of calcium copper titanate ceramics*, J. Am. Ceram. Soc. **88** (2005) 2611-2614.

[13] S. Guillemet-Fritsch, T. Lebey, M. Boulos, B. Durand, *Dielectric properties of $CaCu_3Ti_4O_{12}$ based multiphased ceramics*, J. Eur. Ceram. Soc. **26** (2006) 1245-1257.

[14] L. Ni, X.M. Chen, X.Q. Liu, R.Z. Hou, *Microstructure-dependent giant dielectric response in $CaCu_3Ti_4O_{12}$ ceramics*, Solid State Commun. **139** (2006) 45-50.

[15] C.K. Yeoh, M.F. Ahmad, Z.A. Ahmad, *Effects of Cu and Ti excess on the dielectric properties of $CaCu_3Ti_4O_{12}$ prepared using a wet chemical method*, J. Alloy Compd. **443** (2007) 155-160.

[16] C. Kant, T. Rudolf, S. Drohnos, P. Lukenheimer, S.G. Ebbinhaus, A. Loidl, *Broadband dielectric response of $CaCu_3Ti_4O_{12}$: from dc to the electronic transition regime*, Phys. Rev. B **77** (2008) 045131.

[17] J.J. Liu, C.G. Duan, W.G. Yin, W.N. Mei, R.W. Smith, J.R. Hardy, *Large dielectric constant and Maxwell-Wagner relaxation in $Bi_{2/3}Cu_3Ti_4O_{12}$*, Phys. Rev. B **70** (2004) 144106.

[18] W.T. Hao , J.L. Zhang, Y.Q. Tan, W.B. Su, *Giant dielectric-permittivity phenomena of compositionally and structurally $CaCu_3Ti_4O_{12}$-like oxide ceramics*, **92**

(2009) 2937-2943.

[19] D.C. Sinclair, T.B. Adams, F.D. Morrison, A.R. West, *$CaCu_3Ti_4O_{12}$: One-step internal barrier layer capacitor*, Appl. Phys. Lett. **80** (2002) 2153-2155.

[20] B.A. Bender, M.J. Pan, *The effect of processing on the giant dielectric properties of $CaCu_3Ti_4O_{12}$*, Mater. Sci. Eng. B **117** (2005) 339-347.

[21] J.L. Zhang, P. Zheng, C.L. Wang, M.L. Zhao, J.C. Li, J.F. Wang, *Dielectric dispersion in $CaCu_3Ti_4O_{12}$ at High Temperatures*, Appl. Phys. Lett. **87** (2005) 142901.

[22] S. Krohns, P. Lunkenheimei, S.G. Ebbinghaus, A. Loidl, *Broadband dielectric spectroscopy on single-crystalline and ceramic $CaCu_3Ti_4O_{12}$*, Appl. Phys. Lett. **91** (2007) 022910.

[23] S. Krohns, P. Lunkenheimer, S.G. Ebbinghaus, A. Loidl, *Colossal dielectric constants in single-crystalline and ceramic $CaCu_3Ti_4O_{12}$ investigated by broadband dielectric spectroscopy*, J. Appl. Phys. **103** (2008) 084107.

[24] D.P. Cann, S. Aygun, X. Tan, *Dielectric properties of the distorted perovskite $CaCu_3Ti_4O_{12}$*, pp. 153-156 in Extended Abstract of the 11th US-Japan Seminar on Dielectric and Piezoelectric Ceramics, Sapporo, Japan. September 2003.

[25] I.P. Raevski, S.A. Prosandeev, A.S. Bogatin, M.A. Malitskaya, L. Jastrabik, *High dielectric permittivity in $AFe_{1/2}B_{1/2}O_3$ nonferroelectric perovskite ceramics (A=Ba, Sr, Ca; B=Nb, Ta, Sb)*, J. Appl. Phys. **93** (2003) 4130-4136.

[26] J.R. Li, K. Cho, N. Wu, A. Ignatiev, *Correlation between dielectric properties and sintering temperatures of polycrystalline $CaCu_3Ti_4O_{12}$*, IEEE Trans. Dielectr. Electr. Insul. **11** (2004) 534-541.

[27] G.H. Cao, L.X. Feng, C. Wang, *Grain-boundary and subgrain-boundary effects on the dielectric properties of $CaCu_3Ti_4O_{12}$ ceramics*, J. Phys. D: Appl. Phys. **40** (2007) 2899-2905.

[28] C.G. Koops, *On the dispersion of resistivity and dielectric constant of some semiconductors at audiofrequencies*, Phy. Rev. **83** (1951) 121-124.

[29] R. Mauczok, R. Wernicke, *Ceramic boundary-layer capacitors*, Phillips Tech. Rev. **41** (1983) 338-347.

[30] A.J. Moulson, J.M. Herbert, *Electroceramics: Materials, properties and applications.* Chapman & Hall, London, U.K. 1990.

[31] T.T. Fang, L.T. Mei, H.F. Ho, *Effects of Cu stoichiometry on the microstructures, barrier-layer structures, electrical conduction, dielectric responses, and stability of* $CaCu_3Ti_4O_{12}$, Acta Mater. **54** (2006) 2867-2875.

[32] T.B. Adams, D.C. Sinclair, A.R. West, *Influence of processing conditions on the electrical properties of* $CaCu_3Ti_4O_{12}$ *ceramics*, J. Am. Ceram. Soc. **89** (2006) 3129-3135.

[33] S.A. Prosandeyev, A.V. Fisenko, A.I. Riabchinski, I.A. Osipenko, I.P. Raevski, N. Safontseva, *Study of intrinsic point defects in oxides of the perovskite family: I. Theory*, J. Phys. Condens. Matter **8** (1996) 6705-6717.

[34] S.B. Lee, K. Lee, H. Kim, *The role of the grain boundary on the room temperature resistivity of* $Pb(Fe_{1/2}Nb_{1/2})O_3$, Jpn. J. Appl. Phys. **41** (2002) 5266-5271.

[35] P.R. Bueno, J.A. Varela, E. Longo, SnO_2, *ZnO and related polycrystalline compound semiconductors: An overview and review on the voltage-dependent resistance (non-ohmic) feature*, J. Eur. Ceram. Soc. **28** (2008) 505-529.

[36] F.C. Luo, J.L. He, J. He, J. Hu, Y.H. Lin, *Electric and dielectric properties of Bi-doped* $CaCu_3Ti_4O_{12}$ *ceramics*, J. Appl. Phys. **105** (2009) 076104.

[37] P.R. Bueno, R. Tararan, R. Parra, E. Joanni, M.A. Ramírez, W.C. Ribeiro, E. Longo, J.A. Varela, *A polaronic stacking fault defect model for* $CaCu_3Ti_4O_{12}$ *material: an approach for the origin of the huge dielectric constant and semiconducting*

coexistent features, J. Phys. D: Appl. Phys. **42** (2009) 055404.

[38] J.J. Liu, R.W. Smith, W.N. Mei, *Synthesis of the giant dielectric constant material CaCu3Ti4O12 by wet-chemistry methods*, Chem. Mater. **19** (2007) 6020-6024.

[39] W.X. Yuan, S.K. Hark, W.N. Mei, *Effective synthesis to fabricate a giant dielectric-constant material $CaCu_3Ti_4O_{12}$ via solid state reactions*, J. Ceram. Process. Res. **10** (2009) 696-699.

[40] W.X. Yuan, S.K. Hark, W.N. Mei, *Investigation of the Triple Extrinsic Origins of Colossal Dielectric Constant in $CaCu_3Ti_4O_{12}$ Ceramics*, J. Electrochem. Soc. **157** (2010) G117-G122.

[41] T.T. Fang, C.P. Liu, *Evidence of the internal domains for inducing the anomalously high dielectric constant of $CaCu_3Ti_4O_{12}$*, Chem. Mater. **17** (2005) 5167-5171.

[42] T.T. Fang, H.K. Shiau, *Mechanism for developing the boundary barrier layers of $CaCu_3Ti_4O_{12}$*, J. Am. Ceram. Soc. **87** (2004) 2072-2079.

[43] B.S. Prakash, K.B.R. Varma, *Influence of sintering conditions and doping on the dielectric relaxation originating from the surface layer effects in $CaCu_3Ti_4O_{12}$ ceramics*, J. Phys. Chem. Solids **68** (2007) 490-502.

[44] P. Leret, J.F. Fernandez, J. De Frutos, D.F. Hevia, *Nonlinear I-V electrical behavior of doped $CaCu_3Ti_4O_{12}$ ceramics*, J. Eur. Ceram. Soc. **27** (2007) 3901-3905.

[45] L. Marchin, S.G. Fritsch, B. Durand, *Grain growth-controlled giant permittivity in soft chemistry $CaCu_3Ti_4O_{12}$ ceramics*, J. Am. Ceram. Soc. **91** (2008) 485-489.

[46] C.H. Mu, H.W. Zhang, Y. He, P. Liu, *Influence of temperature on dielectric properties of Fe-doped $CaCu_3Ti_4O_{12}$*, Physica B **405** (2010) 386-389.

[47] C.H. Mu, H.W. Zhang, Y.L. Liu, *Y.Q. Song, P. Liu, Rare earth doped*

$CaCu_3Ti_4O_{12}$ electronic ceramics for high frequency applications, J. Rare Earths **28** (2010) 43-47.

[48] A. Hirata, T. Yamaguchi, *Interfacial reaction of $BaTiO_3$ ceramics with PbO-B_2O_3 classes*, J. Am. Ceram. Soc. **80** (1997) 79-84.

[49] S.-W. Jeong, K.S. Kim, M.T. You, Y. Roh, T. Noguchi, J. Jung, J.-Y. Kwon, *$HfSi_xO_y$-HfO_2 Gate Insulator for Thin Film Transistors*, J. Korean Phys. Soc. **47** (2005) 401.

Chapter 2 Microstructures and dielectric properties of $CaCu_3Ti_4O_{12}$ ceramics synthesized by a wet-chemistry route

The colossal dielectric phenomena in CCTO materials are extrinsic in nature and are generally regarded as MW relaxations occurring at interfaces between samples and the electrodes [1,2-5], depletion layers at domain boundaries [6,7-11], and depletion layers at grain boundaries [2,3,5,12-17]. In addition, nanoscale barrier layer capacitors (NBLC) within CCTO grains, caused by stacking faults [18,19] or strained and composition-disorder boundaries [20], are found to play an important role in explaining observed experimental findings. Because they are located within the CCTO grains, they can be thought of as a kind of domain boundaries. The basic difference between the domain and grain boundaries is that the former have much smaller scale of action compared with the latter. So the NBLC model is also ascribed to as an IBLC model.

Based on the IBLC picture, it is believed that polarization effects at insulating grain/domain boundaries between semiconducting grains/domains generate the colossal dielectric constant values. Charge carriers residing on the interface between electrodes and samples also generate a "surface barrier layer capacitor" (SBLC) (electrode effects), because of the formation of Schottky diodes at the contact-bulk interfaces [1,2-5]. Generally speaking, both IBLC and SBLC take place due to discontinuous change in material distributions. In all, there are three dielectric relaxations due to the extrinsic effects, which are associated with domain boundaries, grain boundaries, and sample surface layers. The first two ones are related with IBLC model, and the other one with SBLC model. Thus we expect to observe them in our studies of CCTO at the same time and at room temperature (RT). Furthermore, based

on our understanding of the previous studies [2,3,5,21-23], the relaxations described in the above-mentioned models were observed and discussed, but never three together at RT. For example, Lunkenheimer *et al.* [2,3] and L. Zhang [5] had performed extensive dielectric measurements of CCTO ceramics, but did not observe any contribution originating from internal domain boundary effects. In the dielectric spectroscopy work of Bueno *et al.* [21,22] and AC conductivity (σ_{AC}) work of Li *et al.* [23], evidences of the existence of three relaxations are apparent in the figures, yet they only recognized and explained two of them. In the case of former, the low-frequency relaxation in Fig. 2 of Ref. [21] and Fig. 1 of Ref. [22] was referred to as grain boundary effects; however, the majority opinion, such as in Refs. [1,4], regarded it as due to electrode effects. These three relaxations are again observed in Figs. 6 and 7 of Ref. [18], a later paper by the same group, but they only interpreted the high-frequency (~4 MHz) and intermediate-frequency (~10 kHz) relaxations as caused by grain boundaries and stacking faults inside grains, respectively. As for the latter's σ_{AC} measurements, in Fig. 3 of Ref. [23] the relaxations at low (3 Hz) and intermediate (630 Hz) frequency regions were referred as contributions from grain boundaries and domain boundaries. However, most studies attributed the low frequency (3 Hz) relaxation to electrode effects [1-3].

In this study, first, we observe that all three dielectric relaxations appear at the same time and at RT. Second, from the measurements of the dielectric properties, we provide insight into the different relaxation mechanisms and propose a convenient method to separate the contributing factors (domain boundaries, grain boundaries, electrodes) through their frequency dependent responses. Third, from the overall σ_{AC}, we derive an understanding of charge migration mechanisms that can also be adopted to delineate the contributions of domain boundaries, grain boundaries and electrodes.

2.1 Experimental

CCTO powder was prepared by a wet-chemistry method. The synthesis process was described in Chapter 1. The powder was pressed into two pellets at a pressure of 40 MPa, which were sintered for 3 h at 900 and 1050 °C in air. The experimental techniques and measurement conditions used were described in Section 1.3.4.

2.2 Results and discussion

2.2.1 XRD measurements

The room temperature XRD patterns of both pellets are shown in Fig. 2.1. All the diffraction peaks were indexed, which shows that both samples are single phase CCTO. Both pellets show distinct (220), (400) and (422) orientations, thus demonstrating a polycrystalline character. There is no change in their crystalline phase compositions by sintering at different temperatures, but the relative intensities of diffraction peaks of the two samples are different.

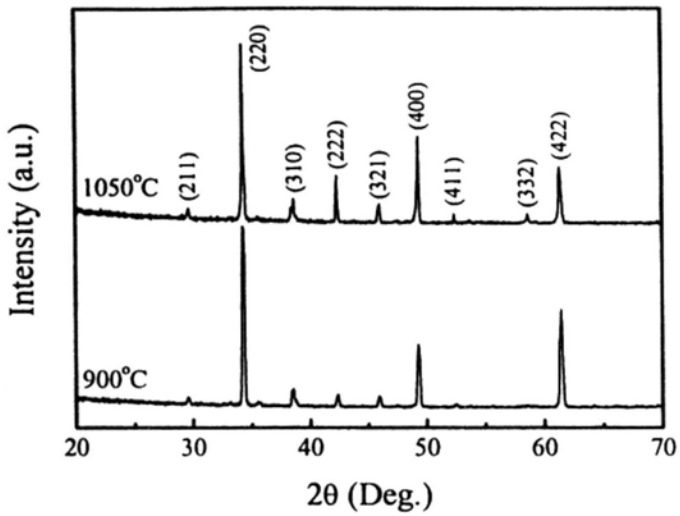

Fig. 2.1 X-ray diffraction patterns of CCTO ceramics sintered at 900 and 1050 °C.

2.2.2 Dielectric measurements

In Fig. 2.2, we plotted the dielectric constant (ε') and loss tangent (D) of our CCTO samples against frequency at two sintering temperatures, 900 and 1050 °C. With careful examination of Fig. 2.2(a), we notice that there are three oscillatory variations over different frequency regions in the measured ε'. At the high frequency region (about 10^6 Hz) ε' declines sharply, but at the low and intermediate frequency regions (below 10^6 Hz) it changes mildly. To support the above-mentioned observations, we further examine the measured dielectric loss D, shown in Fig. 2.2(b), and notice that there are three prominent Debye-like relaxations at low (<40 Hz), intermediate ($\sim 10^4$ Hz) and high ($\sim 10^6$ Hz) frequency regions, which have a one-to-one correspondence with the oscillations in ε'. In fact, it is natural to expect the relaxations to appear more pronounced in D, because it is the ratio of the imaginary and real parts of the dielectric permittivity. For brevity, we shall indicate

them as the 1st, 2nd and 3rd relaxations. We would like to emphasize that these three dielectric relaxations of ceramic CCTO prepared by the wet-chemistry method can be simultaneously observed at RT and are extrinsic origins of the giant ε'. The D peak positions move towards low frequencies with an increase of the sintering temperature. That is to say, higher sintering temperature leads to a lower relaxation frequency, which is the frequency when the dielectric constant starts to decline. At frequencies below the loss peaks, D shows a minimum marking the transition between two next relaxations. The 1st relaxation step closely resembles the Debye-type relaxation [12,13,24]. The 1st and 2nd dielectric relaxations are believed to be explained by IBLC effects based on the Maxwell-Wagner (MW) relaxation mode and can be explained by an equivalent circuit consisting of bulk semiconducting CCTO domains' contribution, which is connected in series to the two parallel *RC* circuits of two different types of internal insulating barrier layers: grain boundaries and domain boundaries [1,23,25].

In Fig. 2.2(a), the plot shows that ε' decreases with the increase of the frequency from 40 Hz to 30 MHz. In addition, both the samples exhibit a very high dielectric constant and the dielectric constant increases with an increase of the sintering temperature. The ceramic pellet sintered at 1050 °C has ε' of ~80,400 at 40 Hz and 40,000 at 1 kHz. For the 900 °C pellet, ε' is about 31,000 at 40 Hz. Considering the reported value ε' = 3,000 at 1 kHz with grain sizes of 1 and 1.3 μm sintered at 1000 °C for 20 h using the polymeric citrate precursor and the organic gel-assisted citrate routes by Jha *et al.* [26] and Brizé *et al.* [27], this 900 °C pellet has much higher dielectric constant 6,200 at 1 kHz, although it was sintered at lower temperature for much less time and has smaller grain size as ~0.3 μm (shown in Fig. 2.4(a)). That is to say, the dielectric constant of CCTO ceramics prepared here is extremely enhanced. In addition, ε' of the 900 °C pellet decreases more sharply than that of the 1050 °C one at

the intermediate frequency region. It is due to the 2nd relaxation, which is determined by the interfacial space charge polarization resulting from that the charge carriers accumulate at the interface between semiconducting CCTO grains and insulating grain-boundary barrier layers [28]. So this kind of polarization is associated with the porosities of the pellets [29]. The 900 °C pellet has smaller grains than the 1050 °C one, which indicates that it has higher porosity and larger number of grain boundaries. As a result, more charge carriers are trapped at grain boundaries due to their high resistivity, which will give rise to stronger interfacial space charge polarization. On the other side, the 1050 °C pellet has much higher ε' at high frequency region than the 900 °C one, which can be explained by the 1st relaxation, the dipolar polarization effect corresponding to self-intertwined domain structures present inside the grains [20,25]. Due to the higher sintering temperature, the 1050 °C pellet has larger grains and domains, rendering stronger dipolar polarization effect. Because the relaxation due to domain boundaries is hardly observed at room temperature, relaxation occurring at grain boundaries would become dominant in the dielectric properties, when internal domains are not well developed within the grains. However, even in fine grains of the 900 °C pellet, the domains are formed the same way as those in large grains of the 1050 °C one.

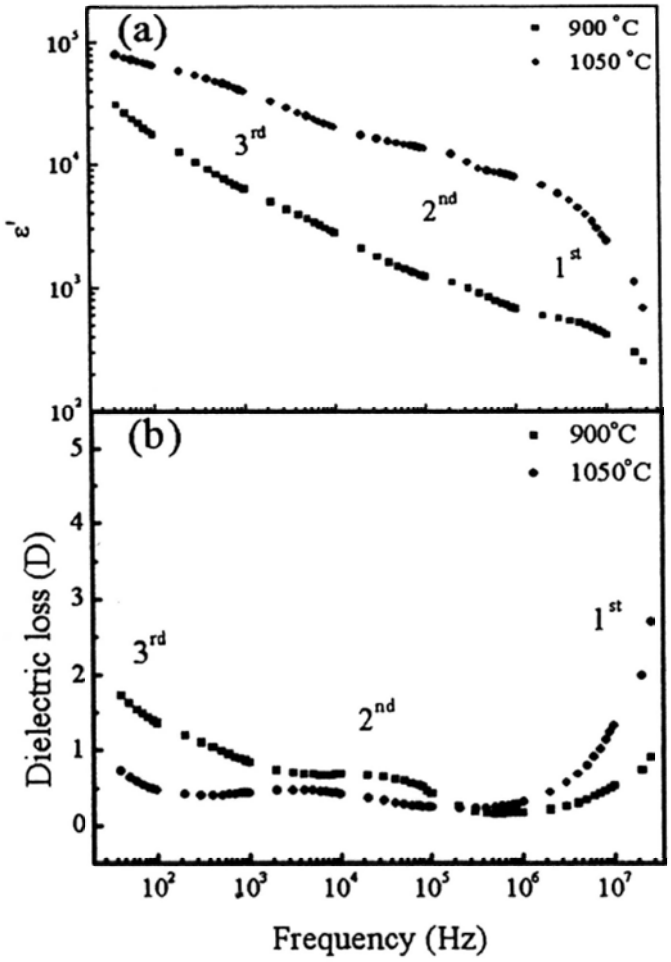

Fig. 2.2 (a) ε' and (b) D *versus* frequency for CCTO ceramics sintered at different temperatures.

In Fig. 2.3, we show the typical dielectric complex diagrams, ε* plots, for our CCTO samples. The analysis of the complex dielectric permittivity is useful for distinguishing distinct relaxation processes and sometimes can be applied to determine different polarization effects that contribute to the entire dielectric response in the measured frequency range. We prefer to adopt the dielectric complex diagram approach rather than the complex impedance diagrams [30,31] following a similar route by Bueno *et al.* [21,22,32], based on the fact that it is more efficient in identifying the origins of dielectric relaxation processes. For example, even though

we obtained only a single semicircular arc within the measured frequency regions through the impedance spectroscopy of our samples (not shown), three successive semicircular arcs are clearly presented in Fig 2.3. For the 900 °C sintered sample, the 1st and 2nd arcs are barely visible in Fig. 2.3(a), so we show an expanded plot of its high frequency region in the inset. Nevertheless, for the 1050 °C sintered sample, the 1st and 2nd arcs are clearly visible. The three arcs in the low, intermediate and high frequency regions can be interpreted by using an equivalent circuit that is composed of three parallel RC elements connected in series, representing three relaxations at different frequencies. The 3rd arc located in the relatively low frequency region is sensitive to surface treatments [33,34], dc electric field [33,34], type of the electrodes [1,2], applied AC voltage [3], which is typical for the electrode relaxation, no doubt it is electrode effects [5]. That is to say, unlike what is said in most reports [5,12,13,17], the resistivity obtained from the intercept on the real axis of the semicircular arc at the low frequency region is not the grain-boundary resistivity but the sample surface resistivity. On the contrary, the 1st and 2nd arcs at high and intermediate frequency regions are more inert to field changes, therefore they are not related to an electrode relaxation phenomenon [33,34]. Both of them are also not intrinsic in origin, because the arc corresponding to intrinsic dielectric relaxation of domains/grains can not be observed at RT, and was only observed at very low temperature (~100 K) as shown in previous studies [12,35]. So, both of them have to be associated with IBLC effects that have more to do with the microstructures of the samples. Therefore, we ascribe them to contributions from grain and domain boundaries; and regard these two kinds of insulating barrier layers as of a similar nature. Since the domain boundaries are contained within the grains, their separations are shorter than those between grain boundaries [21,22]. Hence, the relaxation associated with them occurs at higher

frequency. As a result, the 1st Debye-like relaxation is related to domain boundaries, and is most likely resulted from dipolar relaxations within CCTO grains. Because the dielectric relaxation corresponding to the domain boundaries is clearly revealed in both the CCTO samples with fine (~0.3 μm) and large (~55 μm) grains, the domains are well developed within fine grains as well as large ones, even though the domains were scarcely observed in the fine grains (<2 μm) [20]. Thus the discovery of domains inside the CCTO grains provides a unified picture for the giant dielectric response for both the polycrystalline ceramics and single crystals, because both of them possess domain boundaries that give rise to the 1st relaxation. Following similar arguments, then the 2nd relaxation in the intermediate frequency region has to be ascribed to grain boundaries.

To briefly conclude, we regard that the 1st MW relaxation as related to semi-conducting domains separated by more insulating domain boundaries, the 2nd to semi-conducting grains separated by more insulating grain boundaries, and the 3rd to the formation of a metal-insulator diode, ordinarily called Schottky diodes, at the interfaces between the insulating sample surface layers and the electrodes [1,2-5]. On the basis of aforementioned discussions plus the relaxation associated with bulk CCTO phase (in this case, domains), the equivalent circuit for the dielectric relaxation responses of CCTO is represented by a series of four parallel RC elements, describing the contributions of domains, domain boundaries, grain boundaries and surface layers. Each relaxation has its own characteristic frequency. To be more specific, using the 1050 °C sintered sample as an example, the 1st relaxation associated with domain boundaries occurs at 6 MHz, while the 2nd one associated with grain boundaries at 800 Hz. That is to say, the domain-boundary relaxation is not only clearly seen at RT, but also well separated from the relaxation associated with grain boundaries in this

investigation. The 3rd relaxation due to electrode effects tends to occur at very low frequency, as low as 3 Hz [23], much lower than our lowest measurement frequency of 40 Hz.

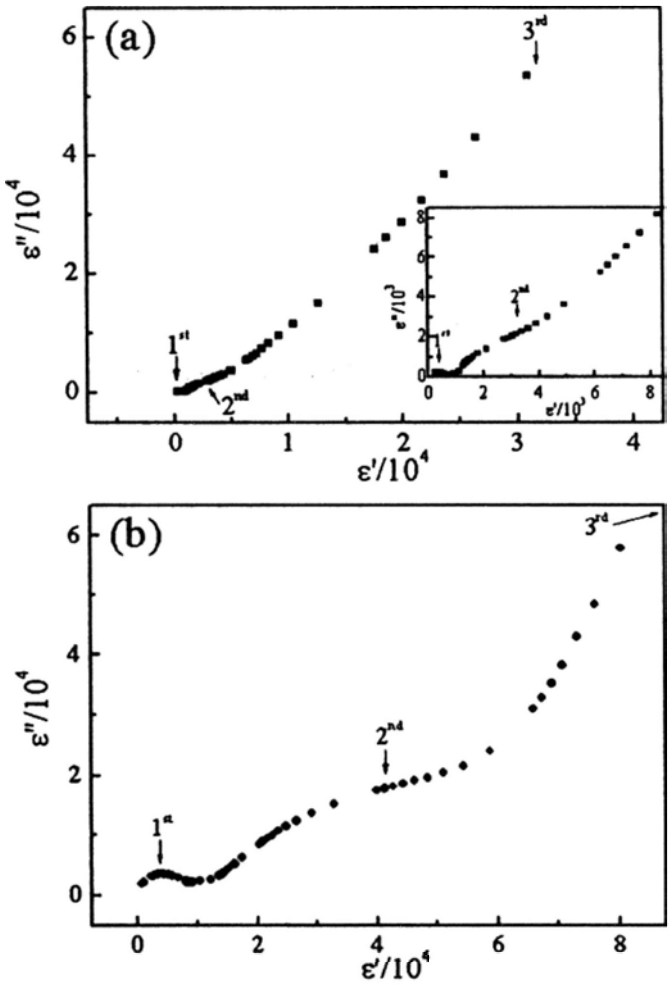

Fig. 2.3 ε* plots (a) and (b) for the 900 °C and 1050 °C sintered CCTO, showing the whole relaxation pattern. The high frequency region exhibits a Debye-like relaxation relating to domain boundary effects, the intermediate frequency one to grain boundary effects and the low frequency one to the electrode effects. The arrows indicate the characteristic frequency of the relaxations. The inset is a magnification of the high frequency region of the 900 °C data.

2.2.3 SEM examinations

The evolution of the microstructures of CCTO ceramics is shown in Fig. 2.4. The

grain size significantly increases with the sintering temperature. More importantly, at a sintering temperature of 900 °C, the sample consists of fine spherical grains with an average size of about 0.3 μm. The grains of the 1050 °C sample, however, have an angular shape with the automatically flat interface and a size distribution in the range of 30-100 μm, and its average grain size is ~55 μm. Even though domains usually develop inside the large grains (> 2 μm) of CCTO [20,36], they have been shown to exist within fine grains as small as ~0.3 μm. Hence, the formation of the domains in such small grains might result from the much finer CCTO powder synthesized by the wet-chemistry method than the conventional solid-state reaction.

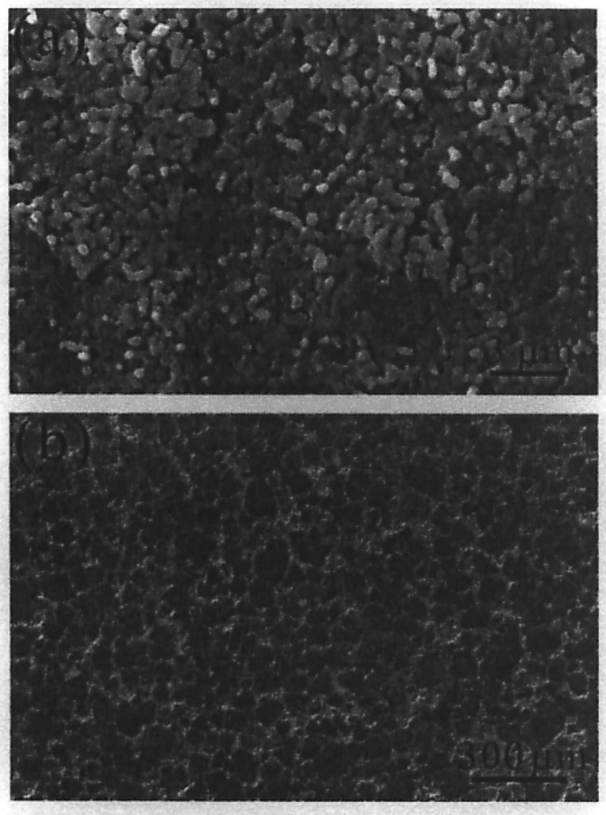

Fig. 2.4 SEM images for CCTO ceramics after sintered at (a) 900 and (b) 1050°C.

2.2.4 AC conductivity

In Fig. 2.5, we show the dependence of AC conductivity (σ_{AC}) of CCTO ceramics.

It can be observed that the conductivities of CCTO ceramics are within the conductivity range of semiconductors. This general picture of conductivity indicates that there are multiple step-like increases as a function of frequency, which is another evidence of the existence of three kinds of insulating barriers in CCTO ceramics and suggests the existence of multiple dielectric relaxation processes. The multiple step-like increases in the middle and high frequency regions are demonstrated to be associated with grain boundaries and domain boundaries, respectively. From the experimental results, the 1050 °C pellet has a higher conductivity, which results from larger density of oxygen vacancies introduced by higher sintering temperature [37,38].

AC conductivity measurements were used to corroborate our dielectric spectroscopy study. Always the conductivity measurement sheds light into different relaxation mechanisms and provides a straightforward way to distinguish different contributing factors through inspecting their frequency dependence, because the different spatial densities of domain and grain boundaries may influence the mobility of the charge carriers at different frequency regions. Hence in Fig. 2.5 we observed multiple variations in AC conductivity spectra of our CCTO. The conductivity starts at low frequencies as σ_{DC}, then increases smoothly and finally becomes dispersive with increasing frequency. Around 10^4 and 10^3 Hz for the 900 and 1050 °C sintered samples, respectively, we observe onsets of an intermediate frequency relaxation. Around 10^7 Hz, a high frequency relaxation starts to occur. By connecting the crossover points at near DC and dispersive conductivities of the two samples, straight lines that divide the AC conductivity-frequency spectra into four regions, labeled as I, II, III and IV in the figure, are obtained. As it turns out, these crossover frequencies coincide with those of dielectric relaxations. We note that the relaxation frequencies

shift to lower values with increasing sintering temperature. Higher sintering temperature reduces the amount of defects and allows grains to grow big, as a result, rendering electronic excitations easier at domain and grain boundaries. The multiple step-like increases in σ_{AC} are generally believed to be caused by a potential well profile with multiple barrier heights [39]. There are reports [5,23] suggesting that these increases are manifestations of multiple relaxation processes that reveal a succession from DC to AC conductivities, which is typical for hopping of localized charge carriers [40]. There are three kinds of insulating barriers in CCTO associated with domain boundaries, grain boundaries and sample surfaces, which can affect conductivity [10,25,41]. Summarizing the above, a clear and complete picture is in order: corresponding to Regions I, II, III and IV, the potential barriers, associated with domain boundaries, grain boundaries and sample surfaces, lead to four frequency-dependent contributions to conductivity: namely, carrier migration localized within domains [23], carrier migration localized within grains [23], carrier migration localized within the samples, long range diffusion of carriers [23], according to the jump relaxation model [42].

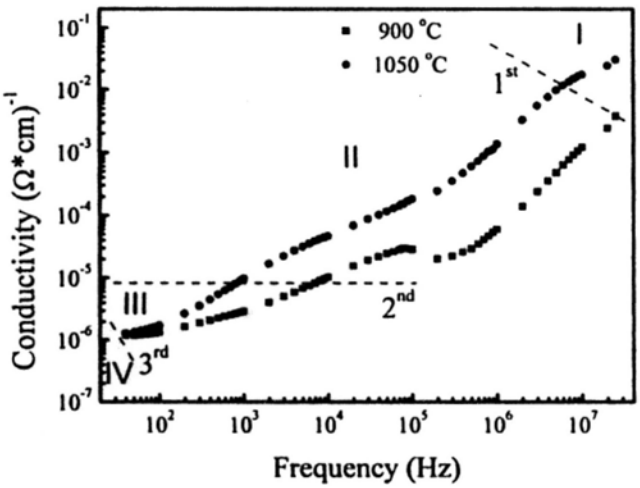

Fig. 2.5 σ_{AC} *versus* frequency for ceramic CCTO at RT.

2.3 Conclusions

$CaCu_3Ti_4O_{12}$ has been successfully synthesized by a wet-chemistry method and calcining route, at relatively lower temperature and in shorter time than the conventional solid-state reaction. The main purpose of this investigation is to directly distinguish three dielectric relaxations resulting from extrinsic origins that render the giant dielectric constant and resolve the conflicts on the resistivity deduced from the impedance spectroscopy. We report complex dielectric spectroscopy and AC conductivity measurements of CCTO ceramics, and observe clearly the occurrence of three relaxations at RT. After close examinations, we conclude that they are caused by dielectric relaxations associated with three kinds of insulating layers at internal domain boundaries, grain boundaries, and sample surfaces. Meanwhile, various mechanisms of the migration of charge carriers, which tend to show different frequency dependence, are manifested in σ_{AC}. Based on the assumption of Schottky diode formation (electrode effects) and IBLC model (domain and grain boundary effects), an entirely interface-related mechanism accounts for not only the observed dielectric relaxations but also the frequency dependent AC conductivity. More specifically, the presence of the domains embedded inside the grains of CCTO ceramics not only elucidates the dielectric responses of the polycrystalline and singe-crystal CCTO, but also justifies that the extrinsic effects are the major causes for enhancing the dielectric response.

References

[1] P. Lunkenheimer, R. Fichtl, S.G. Ebbinghaus, A. Loidl, *Nonintrinsic origin of the colossal dielectric constants in $CaCu_3Ti_4O_{12}$*, Phys. Rev. B **70** (2004) 172102.

[2] S. Krohns, P. Lunkenheimei, S.G. Ebbinghaus, A. Loidl, *Broadband dielectric spectroscopy on single-crystalline and ceramic $CaCu_3Ti_4O_{12}$*, Appl. Phys. Lett. **91** (2007) 022910.

[3] S. Krohns, P. Lunkenheimei, S.G. Ebbinghaus, A. Loidl, *Colossal dielectric constants in single-crystalline and ceramic $CaCu_3Ti_4O_{12}$ investigated by broadband dielectric spectroscopy*, J. Appl. Phys. **103** (2008) 084107.

[4] C.C. Wang, L. W. Zhang, *Surface-layer effect in $CaCu_3Ti_4O_{12}$*, Appl. Phys. Lett. **88** (2006) 042906.

[5] L. Zhang, *Electrode and grain-boundary effects on the conductivity of $CaCu_3Ti_4O_{12}$*, Appl. Phys. Lett. **87** (2005) 022907.

[6] C.C. Homes, T. Vogt, S.M. Shapiro, S. Wakimoto, A.P. Ramirez, *Optical response of high-dielectric-constant perovskite-related oxide*, Science **293** (2001) 673-676.

[7] M.A. Subramanian, A.W. Sleight, *$ACu_3Ti_4O_{12}$ and $ACu_3Ru_4O_{12}$ perovskites: high dielectric constants and valence degeneracy*, Solid State Sci. **4** (2002) 347-351.

[8] L. He, J.B. Neaton, M.H. Cohen, D. Vanderbilt, C.C. Homes, *First-principles study of the structure and lattice dielectric response of $CaCu_3Ti_4O_{12}$*, Phys. Rev. B, **65**, 214112 (2002).

[9] M.H. Cohen, J.B. Neaton, L. He, D. Vanderbilt, *Extrinsic models for the dielectric response of $CaCu_3Ti_4O_{12}$*, J. Appl. Phys. **94** (2003) 3299-3306.

[10] S.Y. Chung, I.D. Kim, S.J.L. Kang, *Strong nonlinear current–voltage behaviour*

in perovskite-derivative calcium copper titanate, Nat. Mater. **3** (2004) 774-778.

[11] M.H. Whangbo, M.A. Subramanian, *Structural Model of Planar Defects in $CaCu_3Ti_4O_{12}$ Exhibiting a Giant Dielectric Constant*, Chem. Mater. **18** (2006) 3257-3306.

[12] D.C. Sinclair, T.B. Adams, F.D. Morrison, A.R. West, *$CaCu_3Ti_4O_{12}$: One-step internal barrier layer capacitor*, Appl. Phys. Lett. **80** (2002) 2153.

[13] T.B. Adams, D.C. Sinclair, A.R. West, *Giant Barrier Layer Capacitance Effects in $CaCu_3Ti_4O_{12}$ Ceramics*, Adv. Mater. **14** (2002) 1321-1322.

[14] B.A. Bender, M.J. Pan, *The effect of processing on the giant dielectric properties of $CaCu_3Ti_4O_{12}$*, Mater. Sci. Eng. B **117** (2005) 339-347.

[15] J.L. Zhang, P. Zheng, C.L. Wang, M.L. Zhao, J.C. Li, J.F. Wang, Dielectric dispersion in $CaCu_3Ti_4O_{12}$ at high temperatures, Appl. Phys. Lett. **87** (2005) 142901.

[16] G.Z. Zang, J.L. Zhang, P. Zheng, J.F. Wang, C.L. Wang, *Grain boundary effect on the dielectric properties of $CaCu_3Ti_4O_{12}$ ceramics*, J. Phys. D: Appl. Phy. **38** (2005) 1824-1827.

[17] J. Li, A.W. Sleight, M.A. Subramanian, *Evidence for internal resistive barriers in a crystal of the giant dielectric constant material: $CaCu_3Ti_4O_{12}$*, Solid State Commun. **135** (2005) 260-262.

[18] P.R. Bueno, R. Tararan, R. Parra, E. Joanni, M.A. Ramírez, W.C. Ribeiro, E. Longo, J.A. Varela, A polaronic stacking fault defect model for $CaCu_3Ti_4O_{12}$ material: an approach for the origin of the huge dielectric constant and semiconducting coexistent features, J. Phys. D: Appl. Phys. 42 (2009) 055404.

[19] M.A. Ramírez, P.R. Bueno, R. Tararam, A.A. Cavalheiro, E. Longo, J.A. Varela, Evaluation of the effect of the stoichiometric ratio of Ca/Cu on the electrical and microstructural properties of the $CaCu_3Ti_4O_{12}$ polycrystalline system, J. Phys. D: Appl.

Phys. 42 (2009) 185503.

[20] T.T. Fang, C.P. Liu, *Evidence of the Internal Domains for Inducing the Anomalously High Dielectric Constant of $CaCu_3Ti_4O_{12}$*, Chem. Mater. **17** (2005) 5167-5171.

[21] P.R. Bueno, M.A. Ramírez, J.A. Varela, E. Longo, *Dielectric spectroscopy analysis of $CaCu_3Ti_4O_{12}$ polycrystalline systems*, Appl. Phys. Lett. **89** (2006) 191117.

[22] P.R. Bueno, W.C. Ribeiro, M.A. Ramírez, J.A. Varela, E. Longo, *Separation of dielectric and space charge polarizations in $CaCu_3Ti_4O_{12}/CaTiO_3$ composite polycrystalline systems*, Appl. Phys. Lett. **90** (2007) 142912.

[23] W. Li, R.W. Schwartz, *ac conductivity relaxation processes in $CaCu_3Ti_4O_{12}$ ceramics: Grain boundary and domain boundary effects*, Appl. Phys. Lett. **89** (2006) 242906.

[24] A.R. West, T.B. Adams, F.D. Morrison, D.C. Sinclair, *Novel high capacitance materials:- $BaTiO_3$:La and $CaCu_3Ti_4O_{12}$*, J. Eur. Ceram. Soc. **24** (2004) 1439-1448.

[25] S.Y. Chung, *Lattice distortion and polarization switching in calcium copper titanate*, Appl. Phys. Lett. **87** (2005) 052901.

[26] P. Jha, P. Arora, A.K. Ganguli, *Polymeric citrate precursor route to the synthesis of the high dielectric constant oxide, $CaCu_3Ti_4O_{12}$*, Mater. Lett. **57** (2003) 2443-2446.

[27] V. Brizé, G. Gruener, J. Wolfman, K. Fatyeyeva, M. Tabellout, M. Gervais, F. Gervais, *Grain size effects on the dielectric constant of $CaCu_3Ti_4O_{12}$ ceramics*, Mater. Sci. Eng. B **129** (2006) 135-138.

[28] H. Birey, *Dielectric properties of aluminum oxide films*, J. Appl. Phys. 49 (1978) 2898.

[29] P. Singh, D. Kumar, O. Parkash, *Dielectric behavior of the system $BaSn_{1-x}Nb_xO_3$ ($x \leq 0.10$)*, J. Appl. Phys. **97** (2005) 074103.

[30] C.J.F. Böttcher, P. Bordewijk, Theory of Electric Polarization: Dielectrics in Time-Dependent Fields (Elsevier, Amsterdam, 1992), Vol. II.

[31] A.K. Jonscher, *Dielectric characterisation of semiconductors*, Solid-State Electron. **33** (1990) 737-742.

[32] P.R. Bueno, J.A. Varela, E. Longo, *Admittance and dielectric spectroscopy of polycrystalline semiconductors*, J. Euro. Ceram. Soc. **27** (2007) 4313-4320.

[33] F.M. Pontes, E.R. Leite, E. Longo. J.A. Varela, E.B. Araujo, J.A. Eiras, *Effects of the postannealing atmosphere on the dielectric properties of (Ba, Sr)TiO_3 capacitors: Evidence of an interfacial space charge layer*, Appl. Phys. Lett. **76** (2000) 2433.

[34] I.P. Raevski, S.A. Prosandeev, A.S. Bogatin, M.A. Malitskaya, L. Jastrabik, *High dielectric permittivity in $AFe_{1/2}B_{1/2}O_3$ nonferroelectric perovskite ceramics (A=Ba, Sr, Ca; B=Nb, Ta, Sb)*, J. Appl. Phys. **93** (2003) 4130-4136.

[35] G.H. Cao, L.X. Feng, C. Wang, *Grain-boundary and subgrain-boundary effects on the dielectric properties of $CaCu_3Ti_4O_{12}$ ceramics,* J. Phys. D: Appl. Phy., **40**, 2899 (2007).

[36] T.T. Fang, H.K. Shiau, *Mechanism for developing the boundary barrier layers of $CaCu_3Ti_4O_{12}$*, J. Am. Ceram. Soc. **87** (2004) 2072-2079.

[37] M.R. Shen, Z.G. Dong, Z.Q. Gan, S.B. Ge, W.W. Cao, *Oxygen-related dielectric relaxation and leakage characteristics of Pt/(Ba,Sr)TiO_3/Pt thin-film capacitors*, Appl. Phys. Lett. **80** (2002) 2538.

[38] L. Fang, M.R. Shen, W.W. Cao, *Effects of postanneal conditions on the dielectric properties of $CaCu_3Ti_4O_{12}$ thin films prepared on Pt/Ti/SiO_2/Si substrates*, J. Appl. Phys. **95** (2004) 6483.

[39] E. Barsoukov, J.R. Macdonald, Impedance spectroscopy Theory, Experiment, and Applications (Wiley, Hoboken, NJ, 2005), 46.

[40] S.R. Elliott, *A.c. conduction in amorphous chalcogenide and pnictide semiconductors*, Adv. Phys., **36**, (1987) 135-217; ibid., *Frequency-dependent loss in amorphous semiconductors*, **31** (1982) 553-637.

[41] S.F. Shao, J.L. Zhang, P. Zheng, W.L. Zhong, C.L. Wang, *Microstructure and electrical properties of* $CaCu_3Ti_4O_{12}$ *ceramics*, J. Appl. Phys., **99**, (2006) 084106-084111.

[42] K. Funke, Debye-Hückel-type relaxation processes in solid ionic conductors: The model, Solid State Ionics, **18-19** (1986) 183-190; Jump relaxation in solid electrolytes, Prog. Solid State Chem. **22** (1992) 111-195.

Chapter 3 Effects of adding PVA binder on dielectric and electric properties of $CaCu_3Ti_4O_{12}$ ceramics

It is observed that CCTO prepared by different methods possesses dielectric constant values that varies from 450 to 300,000 [1-6]; hence it is straightforward to conclude that dielectric constant of CCTO is very sensitive to experimental procedures. Polyvinyl alcohol (PVA), a well-known organic binder, was added to CCTO by several research groups for the purpose of producing more compact samples [7-12]. In the present study, a series of ceramic CCTO samples were prepared with various PVA contents, whose influence on microstructure characteristics, frequency-dependent dielectric properties, AC conductivities, and complex impedance spectra were investigated at room temperature. In addition, we also looked into the effect of PVA addition on the current density-electric field behavior of CCTO ceramics.

3.1 Experimental

CCTO ceramics were prepared by a solid state reaction, the details of which were described in Chapter 1. The formation of a monophase powder was confirmed by X-ray diffraction (XRD). The organic binder PVA, at different weight ratios from 0-8%, was added to the calcined powder to assist the formation of compact samples. Then the powder was uniaxially cold pressed into pellets with a diameter of 1 cm at 4000 psi. Sintering was conducted at 1000 °C for 10 h. The sintered pellets prepared from starting mixtures with different PVA contents, 0, 0.4, 0.8, 2 and 8%, were named as P0-P4 as shown in Table 3.1.

Table 3.1 Dielectric and electric parameters of samples P0-P4.

Sample no.	PVA (wt%)	ε' at 1 kHz	ε' at 100 kHz	α	E_b(V cm^{-1})
P0	0	7383	5510	3.12	324.58
P1	0.4	5911	4798	2.76	237.75
P2	0.8	7074	6018	2.80	243.88
P3	2	6208	5349	2.91	251.03
P4	8	4951	4380	3.34	280.46

The experimental techniques and measurement conditions used were described in Section 1.3.4. In addition, current-voltage (*I-V*) characteristics were also measured by applying DC voltages from 1 V to 30 V on the samples at room temperature.

3.2 Results and discussion

3.2.1 XRD analysis and microstructure

XRD patterns of CCTO ceramics with different PVA additions are shown in Fig. 3.1. Careful analysis reveals that there is a perovskite-like phase, and traces of a secondary CuO phase were also identified.

In Fig. 3.2, from (a) to (e) for samples P0-P4, are the SEM images taken from the as-sintered surface. We noticed that CCTO microstructures were not apparently changed after adding PVA binder. That means, under the current experimental conditions, there is no obvious evidence showing that PVA is capable of modifying the grain growth. To further examine the location of the CuO phase, we took SEM images of the as-sintered and fractured surfaces of P1, selected as examples, and show them in Figs. 3.2 (f) and (g). We notice that the liquid-like brilliant phase is located at grain boundaries of the fractured surface, which indicates that the secondary liquid-like phase existed on the as-sintered sample surface layer and interior, even though the amount of the secondary phase inside the samples is smaller in comparison

with on the surface. We also take a typical EDX diagram of the liquid-like phase, Fig. 3.2(h), showing that there are strong Cu peaks. It is deduced that in the Cu-rich secondary phase the Ca:Cu molecular ratio is 1:17.73, the Cu content is much higher than the CCTO stoichiometric value of 1:3.

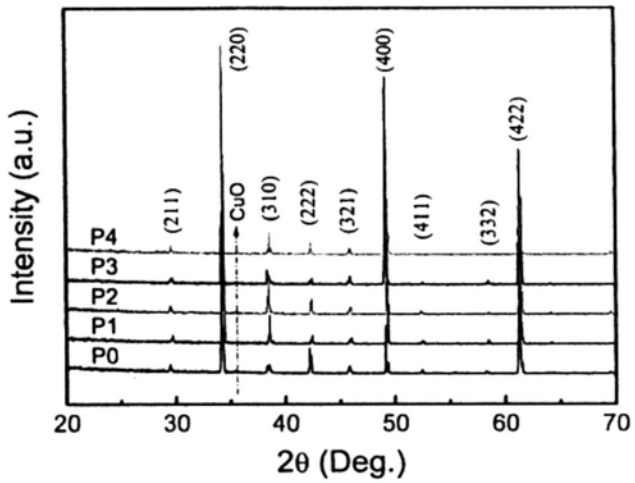

Fig. 3.1 XRD patterns from as-sintered surfaces of samples P0-P4 with different amounts of PVA binder.

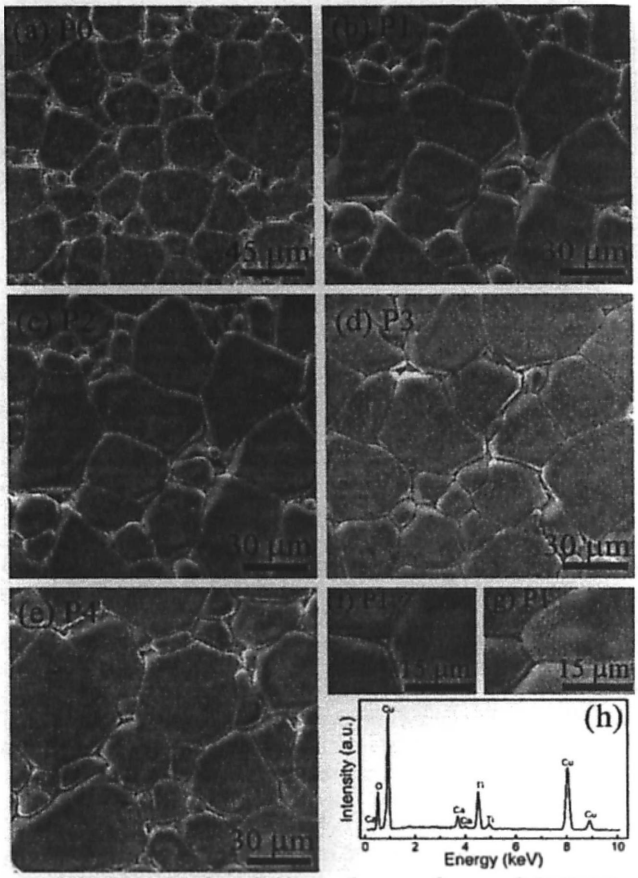

Fig. 3.2 SEM images (a)-(e) obtained from the surface of CCTO ceramics P0-P4. (f) is the magnification of (b) to manifest the grain boundary phase, and (g) is taken from the fractured surface of P1. (h) is typical EDX spectrum of secondary phase.

3.2.2 Dielectric property analysis

The frequency dependence of the dielectric constant (ε') and loss (D) at room temperature for the five samples are shown in Fig. 3.3. We notice that while large differences in ε' show up at the low frequency region, the values of ε' range from 6,000 to 11,000 at 40 Hz, the high-frequency behavior remains similar. We tabulated the ε' values of all the samples at 1 kHz and 100 kHz in Table 3.1. From P1-P4, P2 has the largest ε', and indeed adding more PVA results in smaller ε'. Yet the dielectric constant of P4 is still rather high ~5,000. Moreover, adding the PVA binder weakens the frequency dependence: for example, in case of P0, ε' at 100 kHz is 74.6% of that at 1 kHz, yet for P4, that is about 88.5%. Meanwhile, D decreases with an increase of

PVA binder at the measured frequencies below 10 kHz. In addition, D has the minimum values at different frequencies: 0.093 for P0 at 40 kHz, 0.068 for P1 at 40 kHz, 0.056 for P3 at 20 kHz, 0.045 for P4 at 10 kHz. Though D is not generally influenced by the size of grains and the thickness of grain boundaries, the addition of the PVA binder improves the density of the ceramic pellets, which might result in the smaller D. Basically, the PVA binder provides stable dielectric responses at the low frequency range.

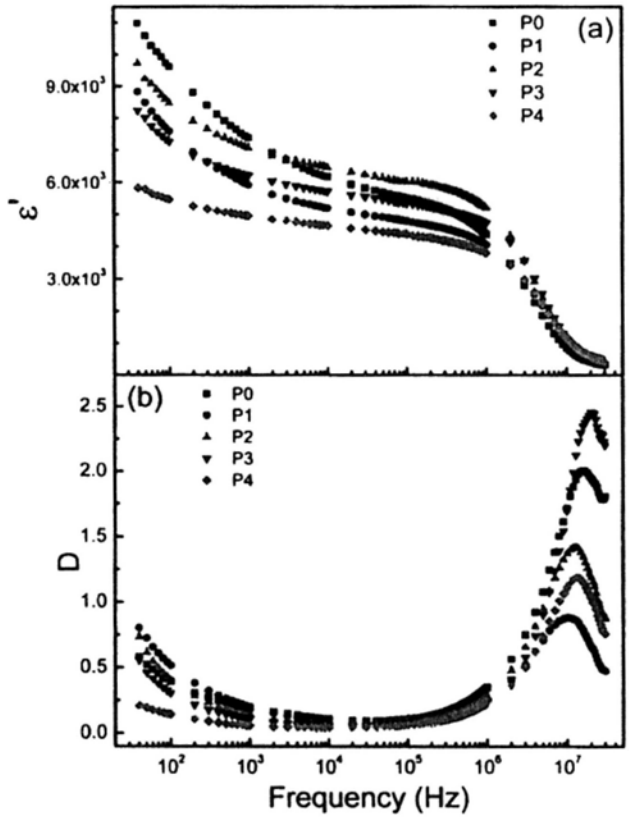

Fig. 3.3 Frequency-dependent (a) ε' and (b) D of P0-P4.

3.2.3 Electric property analysis

In Fig. 3.4, we show the current density-electric field (*J-E*) curves at room temperature for samples P0-P4, which were obtained from the current-voltage (*I-V*) curves after taking into account the diameter and thickness of the samples. Since in

these systems, we expect the relation between J and E to be non-Ohmic, $J \propto E^{\alpha}$, where the nonlinear coefficient α=d*log(J)*/d*log(E)* can be obtained by using linear regression analysis of the *log(J)* versus *log(E)* plot within 0.1-1 mA cm^{-2} range, where it is most non-Ohmic. Conventionally, the breakdown electric field (E_b) was chosen to be the value to cause a 1 mA cm^{-2} current density [10].

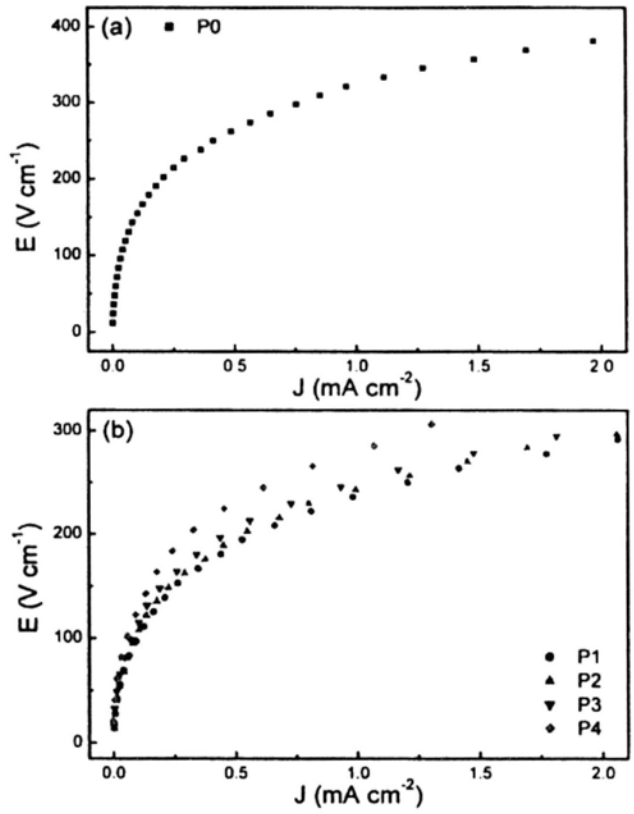

Fig. 3.4 *J-E* curves for samples (a) P0 and (b) P1-P4.

In Table 3.1, we also provide essential data about nonlinear *J-E* behavior of CCTO, such as nonlinear coefficient α and breakdown electric field E_b, which are important parameters for non-Ohmic devices (varistors). Though PVA decomposes rapidly above 200 °C as it undergoes pyrolysis at high temperatures, it does have effect on the electric properties of the samples. We notice that the change of α and E_b values is drastic at first, when small amount (0.4%) of PVA was added. α and E_b values increase from 2.76 to 3.34 and from 237.75 to 280.46 V cm^{-1} with the PVA addition

changes from 0.4 to 8 wt%. All E_b values of samples P1-P4 are smaller than that of P0 (324.58 V cm^{-1}). All these electric characteristics are strongly influenced by the secondary phase located at grain boundaries, particularly as a matter of the thickness of secondary phase between grains, which was explained in detail by Ref. [9]. That is, after adding PVA, the samples are more compact than the pure CCTO ceramics, so the insulating secondary phase at grain boundaries becomes thinner, which reduces the breakdown electric field for all the PVA-added ceramics.

3.2.4 Impedance spectroscopy study

Cole-Cole plots for the complex impedance (Z^*) spectra of P0-P4 are shown in Fig. 3.5. As is conventionally done, we interpret the results using an equivalent circuit consisting of two parallel RC elements in series. One pair of RC elements corresponds to the grain response and the other to the grain-boundary response [13]. The plots at low frequencies in Fig. 3.5(a) present approximately a straight line of progressively increasing slopes from P1 to P4 with increasing PVA contents, which suggest an increase in R_{gb}, the resistivity of grain boundaries. Furthermore, different values of grain resistivity (R_g) for P0-P4 ranging from 60 to 280 Ω cm could be deduced from the diameters of the high-frequency semicircular arcs shown in Fig. 3.5(b). In most cases, we only observe less than half of a semicircle, due to the limitation of the measuring temperature and frequency range.

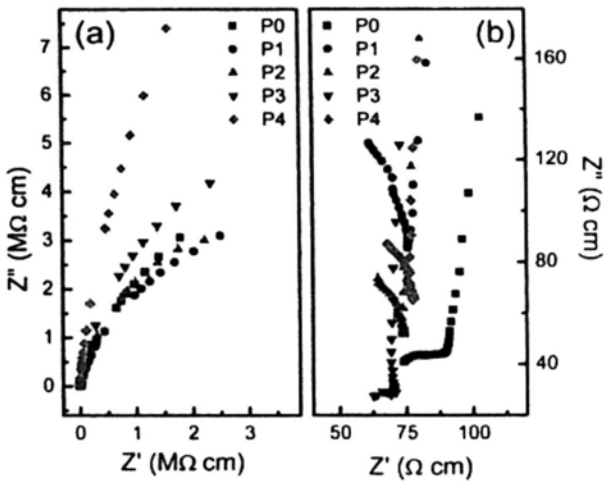

Fig. 3.5 (a) Cole-Cole Z^* plots for P0-P4 at room temperature. (b) shows the enlargement of high-frequency parts of (a).

3.2.5 AC conductivity study

In Fig. 3.6, we exhibit frequency-dependent AC conductivities (σ_{AC}) of samples P0-P4 at room temperature. We notice that the low frequency σ_{AC} of P0-P4 are close in value as shown in Fig. 3.6(a), so we amplify them by plotting log (σ_{AC}) versus frequency in Fig. 3.6(b). Then we realize a strong frequency dependence, indicating hopping of localized charge carriers [14], whereas the dispersion in σ_{AC} is a manifestation of interfacial polarizations that formed because of the inhomogeneous structure. σ_{AC} at low frequencies decreases with increasing PVA, as shown in Fig. 3.6(b). Generally, for all samples, σ_{AC} increases strongly with frequency at the range below 10 MHz, which is the feature of the hopping model, and the transport is dominated by contributions of electron hopping [15]. In a hopping model, different characteristic regions of frequency can be distinguished [16-18]. The conductivity at the lowest frequencies is supposed to be contributed by the sample surface conductivity, which results in electrode effects [17,18]. These effects are formed at the interfaces between sample surfaces and metal electrodes, usually called the Schottky

diode. Due to the decrease of the surface conductivity, electrode effects of P4 became weaker, which renders its dielectric constant lower than the other samples at low frequencies. The main difference between P0 and P1-P4 is the σ_{AC} response at high frequency range above 10 MHz: as we can see that σ_{AC} of P0 increases with the measuring frequencies, because the transport of charge carriers is dominated by contribution from the cluster hopping. Yet for P1-P4, σ_{AC} is saturated at a certain frequency, then declines at high frequencies from 10 to 30 MHz. That is because the fast varying applied field obstructs hopping conduction in more compact structures. This is clearly demonstrated in Fig. 3.6(a).

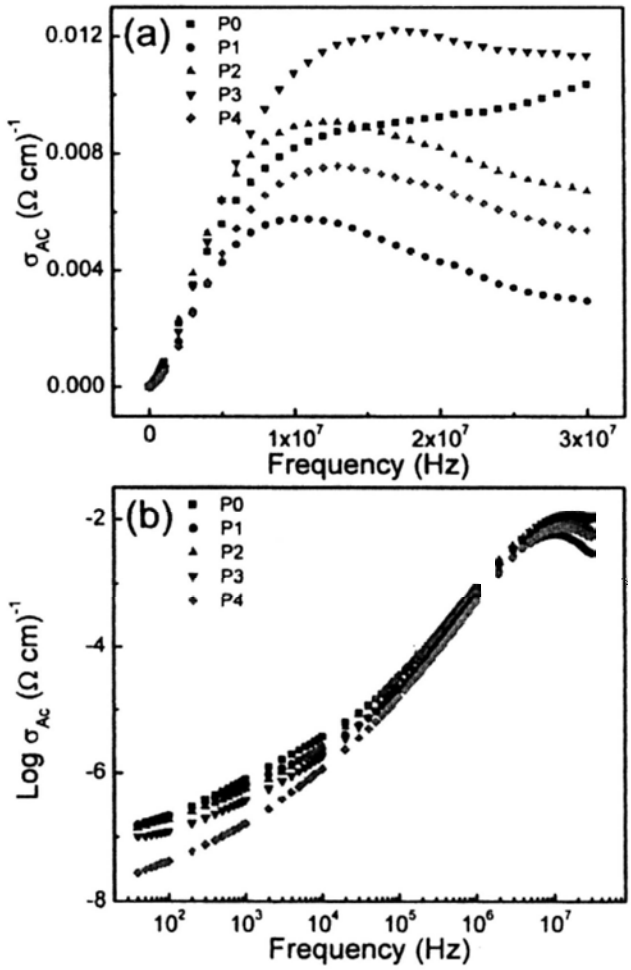

Fig. 3.6 Frequency-dependent σ_{AC} of P0-P4 at room temperature.

3.3 Conclusions

In conclusion, a series of CCTO ceramics were prepared from calcined powder with different amounts of PVA binder in this investigation. The effects of adding the organic binder on microstructures, dielectric and electric properties of high dielectric constant were studied. Adding PVA does not prominently influence the microstructures, yet it modifies the electric and dielectric properties in the following ways. First, it causes a Cu-rich secondary liquid-like phase to reside not only on the surfaces but also between the grains inside the samples, which was not observed in CCTO samples made without using PVA. Second, it stabilizes the frequency dependence response of dielectric constant and reduces the dielectric loss at low frequencies. Third, increase of the PVA content increases the nonlinear coefficient of the *I-V* curves and the breakdown electric field. And fourth, it hinders the hopping of the localized charge carriers. The addition of PVA has a compacting effect to the inhomogeneous structures of CCTO.

References

[1] T.B. Adams, D.C. Sinclair, A.R. West, *Giant barrier layer capacitance effects in $CaCu_3Ti_4O_{12}$ ceramics*, Adv. Mater. **14** (2002) 1321-1323.

[2] D.C. Sinclair, T.B. Adams, F.D. Morrison, A.R. West, *$CaCu_3Ti_4O_{12}$: one-step internal barrier layer capacitor*, Appl. Phys. Lett. **80** (2002) 2153.

[3] M.A. Subramanian, D. Li, N. Duan, B.A. Reisner, A.W. Sleight, *High dielectric constant in $ACu_3Ti_4O_{12}$ and $ACu_3Ti_3FeO_{12}$ phases*, J. Solid State Chem. **151** (2000) 323-325.

[4] R.N.P. Choudhary, U. Bhunia, *Structural, dielectric and electrical properties of $ACu_3Ti_4O_{12}$ (A = Ca, Sr and Ba)*, J. Mater. Sci. **37** (2002) 5177-5182.

[5] P. Jha, P. Arora, A.K. Ganguli, *Polymeric citrate precursor route to the synthesis of the high dielectric constant oxide, $CaCu_3Ti_4O_{12}$*, Mater. Lett. **57** (2003) 2443-2446.

[6] L.C. Kretly, A.F.L. Almeida, R.S. De Olivera, J.M. Sasaki, A.S.B. Soombra, *Electrical and optical properties of $CaCu_3Ti_4O_{12}$ (CCTO) substrates for microwave devices and antennas*, *Microwave Opt. Technol. Lett.* **39** (2003) 145-150.

[7] B.A. Bender, M.J. Pan, *The effect of processing on the giant dielectric properties of $CaCu_3Ti_4O_{12}$*, Mater. Sci. Eng. B **117** (2005) 339-347.

[8] V. Brizé, G. Gruener, J. Wolfman, K. Fatyeyeva, M. Tabellout, M. Gervais, F. Gervais, *Grain size effects on the dielectric constant of $CaCu_3Ti_4O_{12}$ ceramics*, Mater. Sci. Eng. B **129** (2006) 135-138.

[9] P. Leret, J.F. Fernandez, J. De Frutos, D.F. Hevia, *Nonlinear I-V electrical behavior of doped $CaCu_3Ti_4O_{12}$ ceramics*, J. Eur. Ceram. Soc. **27** (2007) 3901-3905.

[10] F.C. Luo, J.L. He, J. Hu, Y.H. Lin, *Electric and dielectric properties of Bi-doped $CaCu_3Ti_4O_{12}$ ceramics*, J. Appl. Phys. **105** (2009) 076104.

[11] C.H. Mu, H.W. Zhang, Y. He, P. Liu, J. Shen, *The origin of multiple dielectric relaxation processes in Fe-substituted $CaCu_3Ti_4O_{12}$ ceramics*, Mater. Sci. Eng. B **162** (2009) 195-199.

[12] L. Ni, X.M. Chen, *Enhanced giant dielectric response in Mg-substituted $CaCu_3Ti_4O_{12}$ ceramics*, Solid State Commun. **149** (2009) 379-383.

[13] S.Y. Chung, *Lattice distortion and polarization switching in calcium copper titanate*, Appl. Phys. Lett. **87** (2005) 052901.

[14] P. Lunkenheimer, R. Fichtl, S.G. Ebbinghaus, A. Loidl, *Nonintrinsic origin of the colossal dielectric constants in $CaCu_3Ti_4O_{12}$*, Phys. Rev. B **70** (2004) 172102.

[15] H.M. Zaki, *AC conductivity and frequency dependence of the dielectric properties for copper doped magnetite*, Physica B **363** (2005) 232-244.

[16] H. Böttger, V.V. Bryksin, *Hopping Conduction in Solids* (Akademie-Verlag, Berlin, 1985).

[17] L. Zhang, *Electrode and grain-boundary effects on the conductivity of $CaCu_3Ti_4O_{12}$*, Appl. Phys. Lett. **87** (2005) 022907.

[18] W.X. Yuan, S.K. Hark, W.N. Mei, *Investigation of the triple extrinsic origins of colossal dielectric constant in $CaCu_3Ti_4O_{12}$ ceramics*, J. Electrochem. Soc. **157** (2010) G117-G122.

Chapter 4 Effects of adding B_2O_3 on dielectric and electric properties of $CaCu_3Ti_4O_{12}$ ceramics

Boric oxide (B_2O_3) is a commonly used glass constituent; it has a low melting temperature ~450 °C, and has a low viscosity at the elevated sintering temperature (1000 °C). As a result, adding B_2O_3 will introduce a continuous grain boundary glassy phase. Prakash *et al.* added directly B_2O_3 powder in weigh ratios of 1, 2, and 3% into a CCTO powder and sintered the mixture at 1000 °C to form ceramic samples. They observed that the low density of B_2O_3 results in an enhancement of the grain size; the dielectric constant increases with increasing amounts of B_2O_3, and the dielectric loss of samples with B_2O_3 added is larger than that of pure CCTO sample.

In this work, to make homogeneous mixtures of B_2O_3 and CCTO, we selected to first dissolve B_2O_3 by ethanol, and then drop the solution into CCTO powders. And also B_2O_3 with different weight ratios of 0.4, 0.8, 2, 5, and 8% was chosen to be mixed with CCTO powder. As a result, the phenomena observed in our samples will be reported later. In the present work, a systematic investigation of the microstructure, electric and dielectric properties of CCTO ceramics as function of B_2O_3 concentration were carried out.

4.1 Experimental

The CCTO powder was prepared by the solid state reaction, using starting materials CuO, TiO_2 and $CaCO_3$ and following procedures described in Chapter 1. After mixing with B_2O_3, in the form of 4 wt% alcohol solution, at weight concentrations ranging from 0.4% to 8%, the obtained powders were pressed into

pellets and sintered at 1000 °C for 10 h.

XRD and SEM of the free surfaces and surfaces with several tens of micrometers polished away of the sintered samples were used to monitor phase changes at room temperature. The experimental techniques and measurement conditions used were described in Section 1.3.4. From EDX measurements, the chemical compositions on the surface and few micrometers below were analyzed. Electric and dielectric measurements were carried out at room temperature.

4.2 Results and discussion

In Fig. 4.1, we show the XRD patterns of the samples. They confirm the formation of single phase CCTO for the samples containing less than 5% B_2O_3. It is also evident that the addition of B_2O_3 brings about undesirable secondary phases of $Cu_3B_2O_6$ and CuO, the corresponding diffraction peaks are indicated by the symbols ! and ^. These peaks start to appear when the B_2O_3 content was increased to 5%. When the concentration of B_2O_3 was increased to 8%, these extraneous peak intensities increase significantly and they were indentified to be a result of the emergence of the CuO phase. Hence, we notice that the addition of B_2O_3 results in the decomposition of CCTO, and brings about the secondary phase CuO. Yet all the XRD peaks from the secondary phase disappears after the samples were polished, indicating that the secondary phase only exists on the surface of the sintered pellets, and this is further confirmed by the SEM images of a fractured surface, as shown in Fig. 4.3.

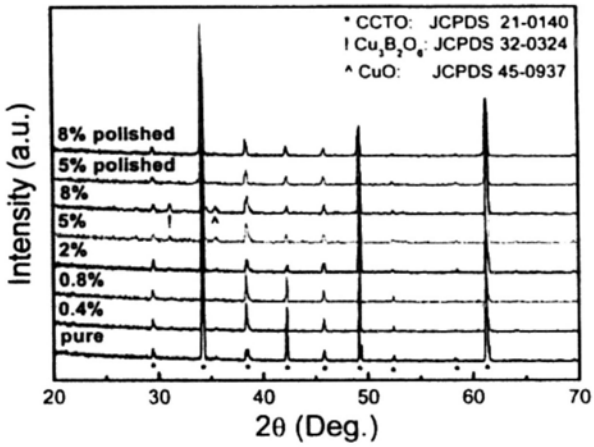

Fig. 4.1 XRD patterns for (a) free surfaces of 0%, 0.4%, 0.8%, 2%, 5% and 8% added samples and (b) polished surfaces of 5% and 8% doped samples.

Microstructures of the pellets containing various amounts of B_2O_3 are depicted in Fig. 4.2. We notice that, after adding B_2O_3, small grains start to show up within the samples. With further increases of B_2O_3, more small grains segregate out and stay between the large grains, resulting in a typically bimodal grain size distribution, i.e. the ceramics are composed of large grains and small grains. Generally, we notice that adding B_2O_3 caused reduction in the average grain size due to appearance of small grains. Hence, based on the IBLC model, we expect a significant change in the dielectric properties of CCTO pellets added with B_2O_3. With continuing increment (5% and 8%) of the glassy B_2O_3 phase, we see further reduction of the grain size, and the morphologies of these two samples are distinctly different from those containing lower B_2O_3. There are indications of the glass phase evolving around CCTO grains, which are particularly clear in the samples containing higher amounts of B_2O_3 (Figs. 4.2 (e) and (f)). The segregation of B_2O_3 especially at grain boundaries hinders the movement of CCTO particles, hence weakens the grain growth. Indeed, for higher concentrations of B_2O_3, most CCTO grains are separated by a thick layer of glassy phase. However, larger amounts (8%-B_2O_3) of the glass phase leads to the increasing grain size. For example, the sample has larger grains than that of 5%. Basically, SEM

micrographs in Fig. 4.2 suggest that the addition of B_2O_3 reduces the grain growth. Especially with 5% and 8% additions, we notice that there are finer grains in the B_2O_3-added CCTO ceramics when compared to the pure CCTO pellet. The addition of B_2O_3 decreases the average grain size when the B_2O_3 concentration is not higher than 5%.

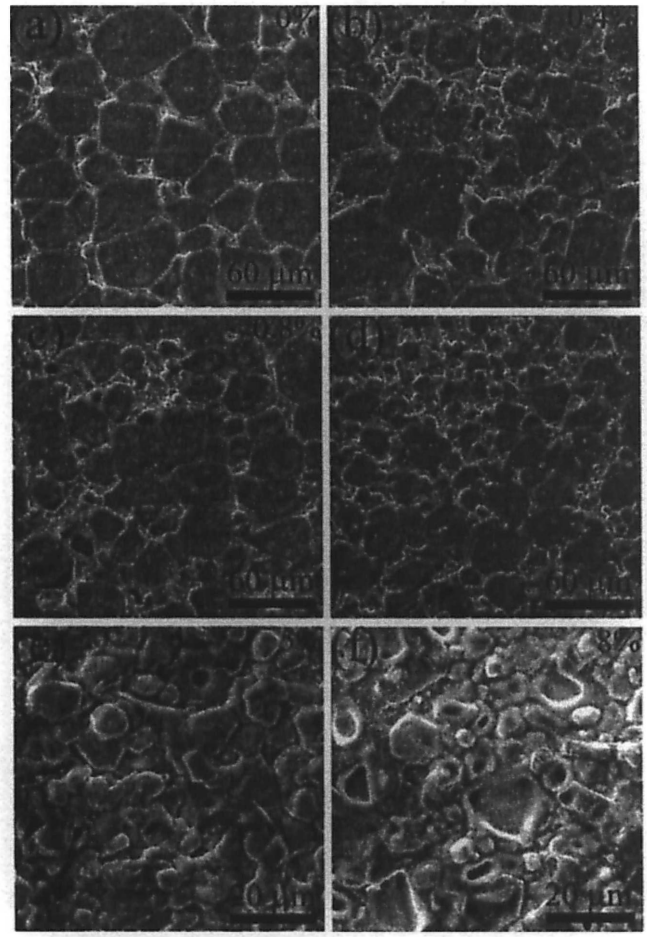

Fig. 4.2 SEM images of free surfaces of CCTO pellets.

In order to detect more definitely the presence of the secondary phase, SEM images were obtained from the fractured surface of the CCTO pellet with 0.4% B_2O_3, selected as a representative. This sample has well defined grain boundaries, and each grain is surrounded by a secondary phase as shown in Fig. 4.3(a). Compared with the pure CCTO phase, the secondary phase is brighter in contrast. Besides the grain

boundaries, it is also found on the surface of the CCTO grains, and there is a secondary phase in the form of a long rod several micrometers in length, such as those shown on the top-left two grains marked by circles in Fig. 3.1(a). The typical EDX spectra of the CCTO and secondary phase are shown in Figs. 4.3 (c) and (d), respectively. Compared with the CCTO phase, the secondary phase is rich in Cu and the Cu/Ca atomic ratio is ~8.64. However, the Cu-rich phase is not noticeable on the fractured surface, as shown in Fig. 4.3(b).

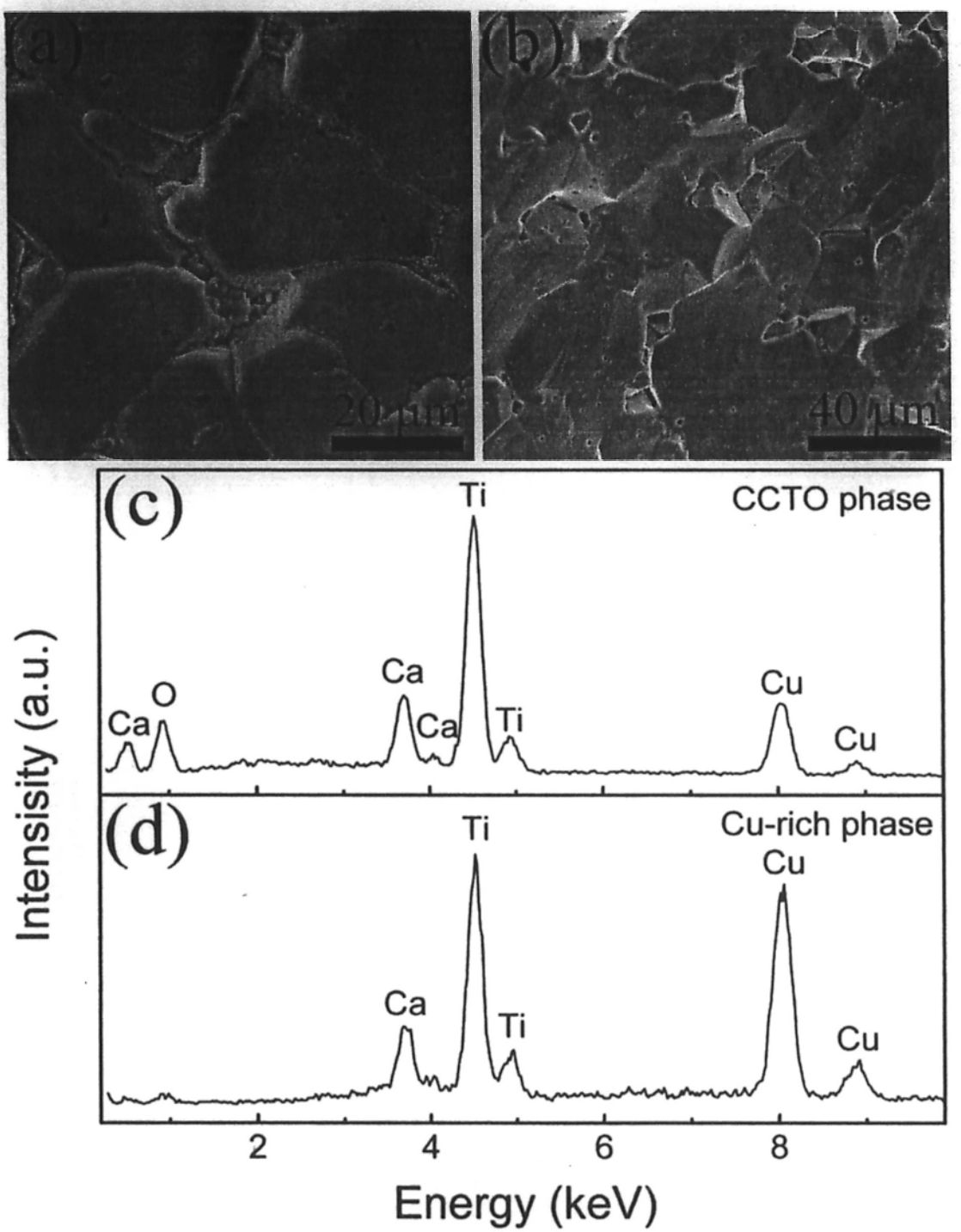

Fig. 4.3 SEM images of (a) the free surface and (b) the fracture surface of 0.4% added CCTO pellet; typical EDX images measured at (c) CCTO phase and (d) secondary phase.

In Fig. 4.4, we show the dependence of the dielectric constant (ε') as a function of frequency of the pure and B_2O_3-added CCTO ceramics. Generally, the dielectric constant changes little with frequency from 40 Hz to 1 MHz, then it decreases

drastically above 1 MHz. We found that the 0.4%-B_2O_3 pellet has the largest low frequency dielectric constant. Based on the IBLC model, the "effective" dielectric constant can be approximated by $\varepsilon' \sim \varepsilon_{gb}(t_g/t_{gb})$ [2], where ε_{gb} is the dielectric constant of the insulating grain boundary phase (~100), t_g is the average grain size and t_{gb} is the average grain boundary thickness. Hence we expect that the dielectric constant deceases with B_2O_3 addition in the region 0.4-5%, where the average grain size was observed to decrease. For the same reason, the pellet containing 8% B_2O_3 has larger dielectric constant than that of the pellet containing 5% B_2O_3. However, we observed that the pure CCTO pellet has larger grains than that of the pellet containing 0.4% B_2O_3, but it has smaller dielectric constant. In addition, although the grains of the pellet containing 2% B_2O_3 (~30 μm) are about 5 times larger than those of the pellet containing 5% B_2O_3 (~6 μm), it has ~1.5 times larger dielectric constant. Therefore, to resolve these seemingly conflicting results, we resort the above phenomena to the IBLC model and attribute them to the decrease of grain-boundary thickness. Even though we did not physically measure it, but it is natural to assume that smaller grains will have thinner boundaries. Yet we believe that it is necessary to examine the thickness of grain boundaries experimentally, such as utilizing a high-resolution transmission electron microscopy, in order to confirm our statements put forth here.

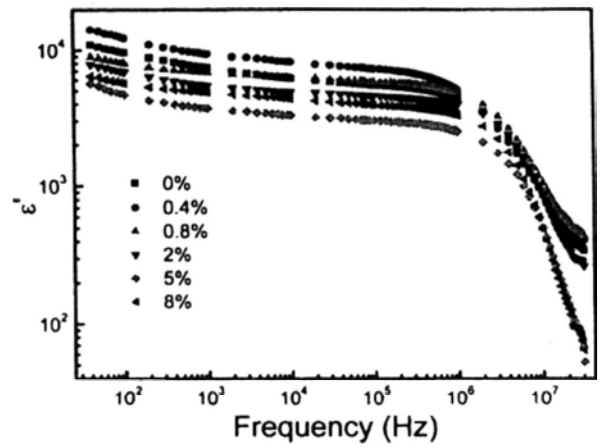

Fig. 4.4 Dielectric constant of CCTO pellets with various B_2O_3 additions.

As shown in Fig. 4.5, we found that at low frequencies, the dielectric loss (D) has little to do with the B_2O_3 addition, but it is enhanced greatly at high frequencies, especially for the pellets containing 5% and 8% B_2O_3. We notice that for each sample, the drop in ε' at high frequencies is accompanied by a rapid increase in D. Just as for the pure CCTO sample, each B_2O_3-added sample has a Debye-like relaxation peak at 1-10 MHz, whose frequency shifts to lower and then returns to higher values. The relaxation is shifted to a higher frequency, implying that more B_2O_3 tend to reduce the activation energy of polarization. We chose the dielectric loss values at 1 kHz of our B_2O_3-added samples to gauge the changes at low frequencies, which are as following: for the two low concentrations, 0.4% and 0.8%, the dielectric loss first decreases from 0.194 to 0.101; for the higher concentration, 2%, it increases to 0.161; with an even higher concentration, 2%-8%, it decreases to 0.105 again. The minimum values of dielectric loss (D_{min}) are listed in Table 4.1. The smallest value among them is 0.061 obtained from the pellet containing 2% B_2O_3 at 30 kHz.

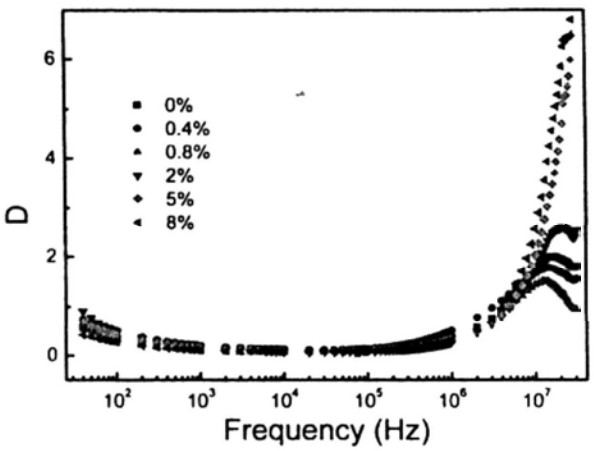

Fig. 4.5 Dielectric loss of CCTO pellets with various B_2O_3 additions.

In Fig. 4.6, we present the Cole-Cole plot to show Z'' versus Z', which are the imaginary and real parts of the impedance Z^* of the pellets containing various amounts of B_2O_3. We notice clearly that only one semicircle corresponding to by grain boundaries response is clearly observed due to the fact that R_g (C_g) << R_{gb} (C_{gb}) and the frequency range limitation of measurement. R_g (C_g) and R_{gb} (C_{gb}) are the resistance and capacitance of grains and grain boundaries. It can be seen from the diameter of the low-frequency arc related to the R_{gb} value, that adding B_2O_3 has influenced the impedance characteristics of the grain and grain boundary, especially the latter.. The semicircles in the low frequency range change obviously with the adding of B_2O_3. R_{gb} first increases for the samples containing 0.4% and 0.8% B_2O_3, and then abruptly decreases in the pellet containing 2% B_2O_3. When the B_2O_3 concentration exceeds 2%, R_{gb} starts to increase. All these can be interpreted as the interplay between the reduction of grain size and grain-boundary thickness. It can be seen that the volume occupied by the grain boundaries increases when the grain size is reduced, thus give rise to the increases in the grain-boundary resistivity. On the other hand, based on our previous deduction, small grains tend to have thinner grain boundaries, which implies lower grain-boundary resistivity. Therefore, these two

trends produce opposite effects in effective dielectric constant. Additional experimental investigations on the change of grain-boundary thickness are required to resolve this intriguing issue. As shown in the inset, the non-zero intercept on the Z'-axis gives the R_g value. It is seen that R_g values for the pure and B_2O_3 added ceramics are 80-140 Ω cm, and the lowest and highest values are obtained from the pellets containing 0.8% and 5%B_2O_3, respectively. And both the pellets containing 5% and 8% B_2O_3 have large grain resistivity values ~120 and 140 Ω cm. This could be explained from the viewpoint of oxygen vacancies [3,4], which is closely related to conducting carriers. It is reasonable to assume that the addition of B_2O_3 (5% and 8%) surrounds the CCTO grains and prevents the formation of oxygen vacancies from escaping, resulting in the R_g increase.

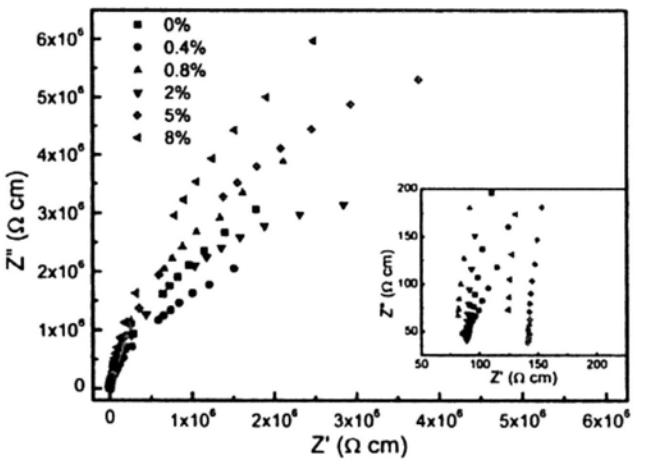

Fig. 4.6 Cole-Cole plots for impedance diagrams of CCTO pellets with various B_2O_3 additions. The inset shows the enlargement of high-frequency parts.

To further study the electric conduction of our samples, in Fig. 4.7, we present the current density-electric field (J-E) characteristic. It is not difficult to see that the samples have a non-Ohmic property. We deduced their nonlinear coefficients (α) and breakdown electric fields (E_b) and listed them in Table 4.1. With increasing B_2O_3, E_b first decreases until 2% B_2O_3 was added, and then it increases. With the B_2O_3 increase, the nonlinear coefficient drops from 3.15 to 2.16. The nonlinear coefficient of the pure

CCTO sample is the largest among all the samples. The breakdown voltage rises when the grain size decreases, as a result of the changes in grain-boundary resistivity.

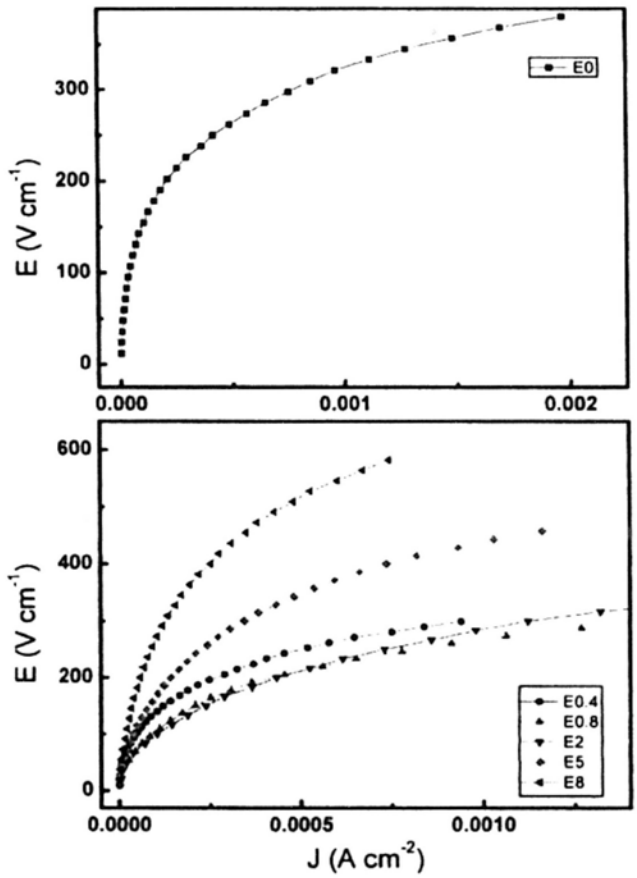

Fig. 4.7 *J-E* plot for CCTO pellets with various B_2O_3 additions.

Table 4.1 Values for the nonlinear coefficient (α), breakdown electric field (E_b) and minimum dielectric loss (D_{min}) of the samples.

B_2O_3 (wt%)	α	E_b(V cm^{-1})	D_{min}
0	3.15	324	0.093
0.4	2.89	304	0.115
0.8	2.50	277	0.068
2	2.29	287	0.061
5	2.24	440	0.071
8	2.16	618	0.077

4.3 Conclusions

A series of B_2O_3-added CCTO ceramics were synthesized by solid sate reaction of

the CCTO powder mixed with different weight ratios of B_2O_3. We performed measurements on their microstructure and electric properties. From SEM images, we observed that adding B_2O_3 promotes a reduction of the grain size, which in turn leads to a decrease of the dielectric constant. Besides the grain size, the addition of B_2O_3 is believed to also cause a reduction of the grain-boundary thickness, which explains the grain-boundary resistivity changes. In addition, adding B_2O_3 also reduces the nonlinear coefficient from 3.15 to 2.16. Correspondingly, the breakdown electric field is also influenced. An internal barrier layer capacitance model was invoked to correlate the dielectric constant with the grain size and grain-boundary thickness in these samples.

References

[1] B. S. Prakash, K. B. R. Varma, *Effect of the addition of B_2O_3 and BaO-B_2O_3-SiO_2 glasses on the microstructure and dielectric properties of giant dielectric constant material $CaCu_3Ti_4O_{12}$*, J. Solid State Chem. **180** (2007) 1918-1927.

[2] T.T. Fang, L.T. Mei, H.F. Ho, *Effects of Cu stoichiometry on the microstructures, barrier-layer structures, electrical conduction, dielectric responses, and stability of $CaCu_3Ti_4O_{12}$*, Acta Mater. **54** (2006) 2867-2875.

[3] L. Fang, M.R. Shen, W.W. Cao, *Effects of postanneal conditions on the dielectric properties of $CaCu_3Ti_4O_{12}$ thin films prepared on $Pt/Ti/SiO_2/Si$ substrates*, J. Appl. Phys. **95** (2004) 6483.

[4] F. Amaral, C.P.L. Rubinger, L.C. Costa, M.A. Valente, R. Moreira, *Enhanced dielectric response of GeO_2-doped $CaCu_3Ti_4O_{12}$ ceramics*, J. Appl. Phys. **105** (2009) 034109.

Chapter 5 Effects of adding HfO_2 on microstructures and dielectric properties of $CaCu_3Ti_4O_{12}$ ceramics

With the frequency- and temperature-independent high dielectric constant [1-4], CCTO has large potential applications in the minimization of microelectronic equipment, such as Dynamic Random Access Memories [5-7] and microwave devices [8]. Yet one main problem for its technical use is the large dielectric loss. So the purpose of the present work is to reduce the loss by mixing it with other low loss high dielectric-constant materials, such as HfO_2. HfO_2 is an intrinsic high dielectric-constant material of $\varepsilon' \sim 25$ [9], whereas for CCTO, the mechanism responsible for the extremely high dielectric constant is understood as extrinsic [1-4]. Thus it is by itself an interesting and challenging project to investigate the dielectric properties of the mixtures.

In the present study, the preparation and characterization of CCTO-HfO_2 ceramics are reported. Specifically, the effects of adding HfO_2 on microstructures and dielectric properties of the ceramics are also reported here.

For illustrative purposes, we divided the following into two parts: in PART A, we discussed a series of CCTO-HfO_2 ceramics containing different HfO_2 weight ratios from 0% to 70%; in PART B, we focused on those CCTO-HfO_2 ceramics of high HfO_2 weight ratios from 20% to 70%, and demonstrated that those dielectric constant satisfied the Lichtenecker's law.

5.1 Experimental

The CCTO powder was synthesized using $CaCO_3$, CuO and TiO_2 by the solid

state method as described in Chapter 1. Appropriate amounts of HfO_2 were added to prepare the CCTO-HfO_2 ceramics. Different weight ratios of HfO_2 ranging from 1% to 70%, more specifically 1%, 2%, 5%, 8%, 10%, 20%, 30%, 50%, and 70%, were added to the CCTO powder, and the mixture was ground for 20 min by hand. Then a pure CCTO, the CCTO-HfO_2 mixtures, and pure HfO_2 were pressed into pellets and sintered at 1000 °C for 10 h.

The experimental techniques and measurement conditions used were described in Section 1.3.4.

PART A

In this part, we mainly discussed a series of CCTO-HfO_2 ceramics containing different HfO_2 weight ratios from 0% to 70%. Their crystalline structures and microstructure evolution and dielectric properties were investigated in detail.

5.2 Results and discussion

The XRD patterns of representative samples are shown in Fig. 5.1. The CCTO diffraction patterns marked with "*" match those in the JCPDS file No. 75-2188, and the others are due to a monoclinic HfO_2 phase (JCPDS No. 74-1506). In fact, the XRD analysis confirms the presence of CCTO as a single phase for HfO_2 concentration up to 5%. For the sample containing 8% HfO_2, we notice in the XRD pattern there is a clear presence of a secondary phase identified as HfO_2. With increasing amounts of HfO_2, its own diffraction peaks become strong. At the same time, the relative intensities of the CCTO peaks are also changed.

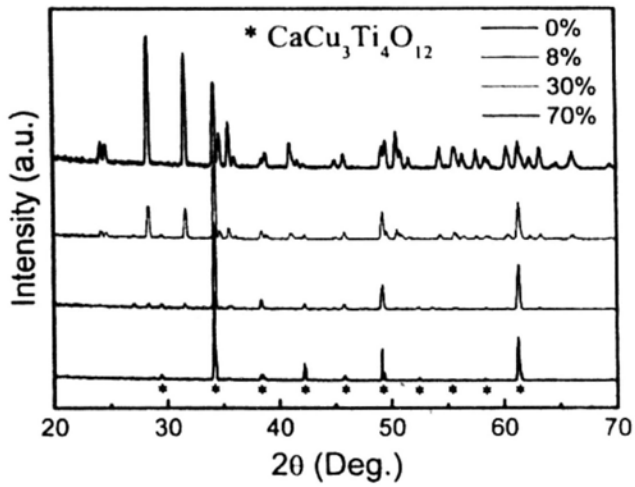

Fig. 5.1 XRD patterns for ceramic samples with different weight ratios.

In Fig. 5.2, we show the typical SEM micrographs of as-sintered surfaces of samples with representative HfO_2 weight ratios. As we can see, the morphologies change significantly after adding HfO_2. We notice that the pure CCTO sample has the largest grains (Fig. 5.2(a)), and the CCTO-HfO_2 ceramics have the bimodal grain size distribution. After adding HfO_2, there exist two classes of CCTO grains of different sizes: one class has a small grain size of several micrometers, and the other has a large grain of size in the order of several tens of micrometers. When the HfO_2 weight ratio is larger than 10%, the grain size becomes evenly distributed. Meanwhile, no clear presence of HfO_2 phase is observed until the HfO_2 addition increases to 8%, and there are small bright grains embedded within large CCTO grains as shown in Fig. 5.2(c). When more HfO_2 is added from 20% to 70%, more bright grains show up, and start to aggregate between the CCTO grains as shown in Figs. 5.2 (e) and (f). In addition, when the bright grains increase in size, the size of CCTO grains reduces greatly. All the bright grains found within and between CCTO grains are confirmed as HfO_2 by using Energy Dispersive X-ray analysis (not shown here). Generally, the average grain size of CCTO-HfO_2 ceramics becomes smaller than that of the pure CCTO

sample. More specifically, from 1 to 8%, the average grain size slightly increases, and then decreases fast from 10 to 70%.

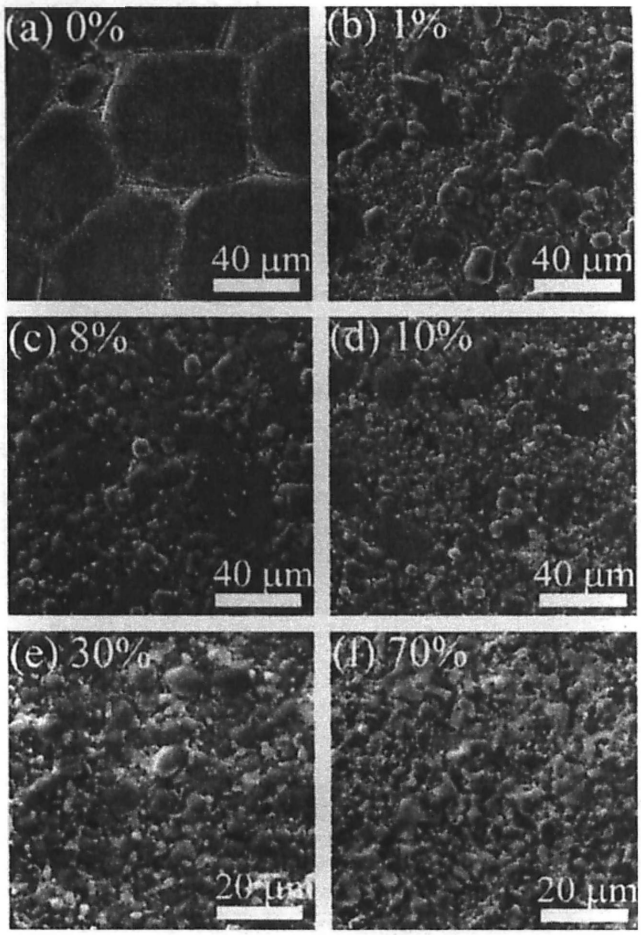

Fig. 5.2 SEM micrographs of CCTO-HfO_2 ceramics with different HfO_2 weight ratios.

In Fig. 5.3, we present the frequency dependence of dielectric constant (ε') and loss (D) of several selected samples. All of them have a large dielectric constant, especially the pure CCTO sample (ε'~10^4). In Fig. 5.3(a), the familiar strong relaxation steps are observed at about 1 MHz. Correspondingly, peaks in the dielectric loss appear, as shown in Fig. 5.3(b). All these curves exhibit the well-known Maxwell-Wagner relaxation, the only difference is the value of ε' decreases after adding HfO_2.

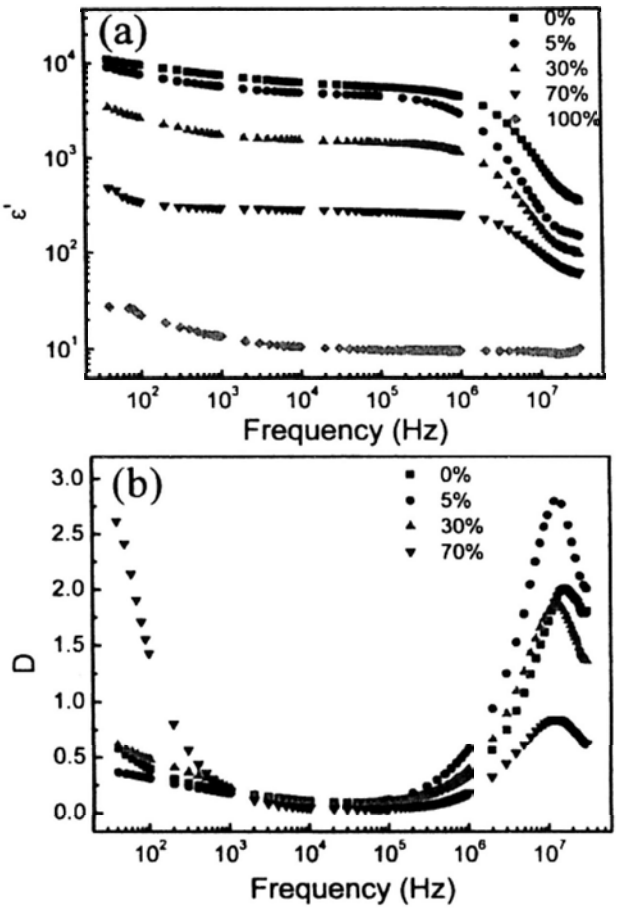

Fig. 5.3 Frequency-dependent (a) ε' and (b) D for CCTO samples with different HfO_2 weight ratios.

In Fig. 5.4, we present ε' and D at 100 kHz for different HfO_2 concentrations. We notice that the pure CCTO sample has the largest dielectric constant. Then ε' drops slightly at low density (1%) addition of HfO_2, then rises up until 10% addition of HfO_2. Afterward the dielectric constant declines to ~270, which is small compared to that of CCTO, but much larger than that of the pure HfO_2 (~9.7). We believe this interesting dielectric behavior has intriguing connection with the appearance of the micron size HfO_2 grains at 8-10%, Figs. 5.3 (c) and (d), and their interactions with the CCTO grains. Thus, the peak at 10% in Fig. 5.4(a) signifies a "local order" of dipoles in the 10%-HfO_2 sample. Then ε' decreases monotonically to a lower value after adding more HfO_2 and gradually reaches the bulk value of HfO_2. To verify the above

mentioned scenario, we have to perform in-depth study of the HfO_2 grain structure, dielectric properties and its interactions with CCTO grains, which is an interesting subject. At the same time, we also notice that, in Fig. 5.4(b), D also varies in a fashion similar to that of ε', except the peak occurs at 5% concentration. Adding 70% HfO_2, D reaches the value of 0.0375, as expected, because most of the insulating HfO_2 grains aggregate and link up as shown in Fig. 5.3(f). The minimum value of the dielectric loss ~0.035 is obtained from the 70%-HfO_2 sample at the frequency of 40 kHz.

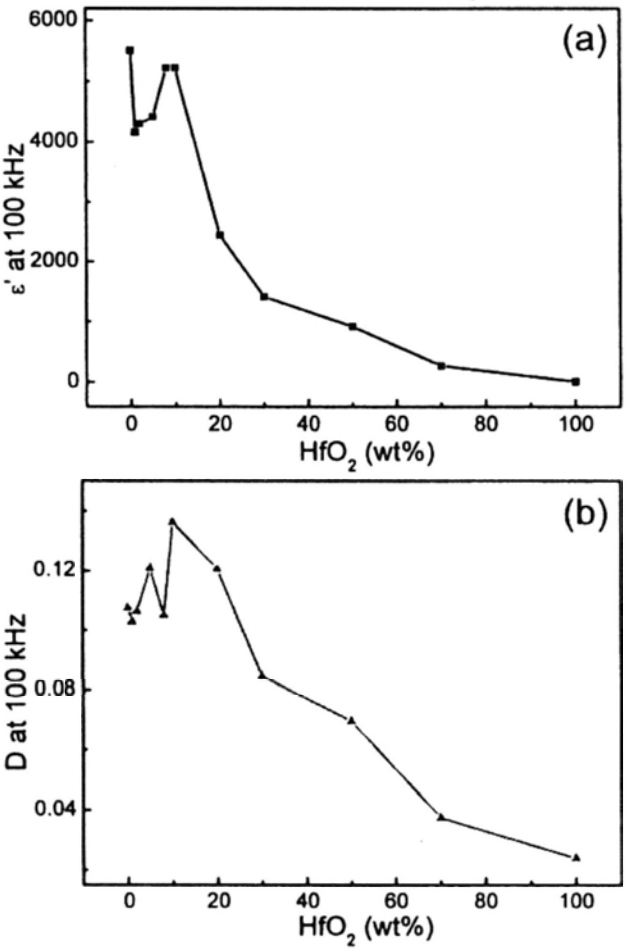

Fig. 5.4 (a) ε' and (b) D at 100 kHz of CCTO-HfO_2 ceramics.

5.3 Conclusions

High dielectric constant ceramics were prepared by mixing HfO_2 and

$CaCu_3Ti_4O_{12}$ (CCTO) powders and sintering at 1000 °C for 10 h. Effects of HfO_2 addition on the microstructures and dielectric properties of CCTO ceramics were investigated. In general, the dielectric constant first drops at low concentration of HfO_2 (1%), then increases with additional amounts up to 10%, and then decreases monotonically all the way for up to 70%, at which point the dielectric constant still remains large (~270) at 100 kHz. Furthermore, the dielectric loss is also influenced by adding HfO_2, and the lowest value of 0.035 was obtained at 40 kHz from the sample containing 70% HfO_2. Hence with proper mixing and thorough investigation, we are able to monitor the dielectric properties of the CCTO-HfO_2 composite materials, which may lead to desired applications in microelectronics.

PART B

In this part, we mainly discuss the dielectric properties of CCTO-HfO_2 ceramics containing high HfO_2 weight ratios from 20% to 70%. There are obvious differences between these samples from those with low HfO_2 concentrations, namely the CCTO grains are small in size and distribute homogenously through out the samples.

5.4 Results and discussion

In Fig. 5.5, we show the XRD patterns obtained from the ceramics with different HfO_2 weight ratios at room temperature. The pure CCTO sample is polycrystalline and of single phase. All the CCTO diffraction peaks are marked by *, and the other

peaks corresponding to HfO_2 are clearly noticeable, and become stronger with increasing HfO_2 content. In order to supply a reference diffraction pattern, the XRD pattern of the pure HfO_2 ceramic sintered under the same condition is also shown in Fig. 5.5. In any case, the CCTO phase is predominant in the XRD patterns of all the samples with HfO_2 addition.

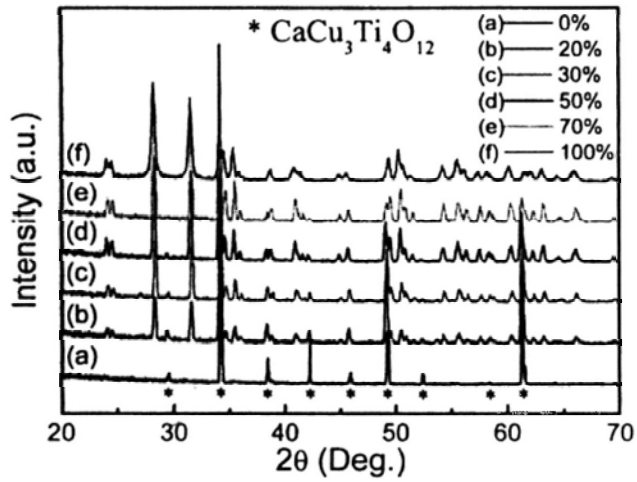

Fig. 5.5 XRD patterns of CCTO-HfO_2 ceramics for different HfO_2 weight ratios.

The SEM images of the prepared ceramics containing various weight percents of HfO_2 are shown in Fig. 5.6. Note that the magnifications of the first two images are different from the rest, because the grain size changes drastically at high HfO_2 concentrations. For comparison, the low and high magnification SEM images of the pure CCTO ceramic are shown in Figs. 5.6 (a) and (b). In the pure CCTO sample, we can see that the average size of the large grains is about 15 μm, whereas, the small grains are about 5 μm, and the largest ones are about 60 μm (Fig. 5.6(b)). After adding 20% HfO_2 (Fig. 5.6(c)), the CCTO grains are reduced to an average size of about 3 μm. It is necessary to notice that CCTO grains are dark in contrast and the

HfO_2 grains are relatively brighter. At first, in the sample containing 20% HfO_2, there are small, less than 1 μm, HfO_2 grains between the CCTO grains. Then the amount of such grains increases a lot in the sample containing 30% HfO_2 (Fig. 5.6(d)). In addition to the concentration increase, the HfO_2 grain size increases to ~2 μm in the sample containing 50% HfO_2 (Fig. 5.6(e)). Finally, in Fig. 5.6(f), we can see that HfO_2 grains have aggregated with each other to form multiple-connected large grains. Since HfO_2 is insulating, it is difficult for us to obtain very clear SEM images form the pure HfO_2 sample. Mostly, we observe that the HfO_2 grains are homogeneously distributed between the CCTO grains in CCTO-HfO_2 ceramics. On top of that, adding more HfO_2 enhances the segregation of CuO, and CuO liquid-like layers with the thickness about 1 μm locate between CCTO grains, which are marked by circles in Figs. 5.6 (c) and (d).

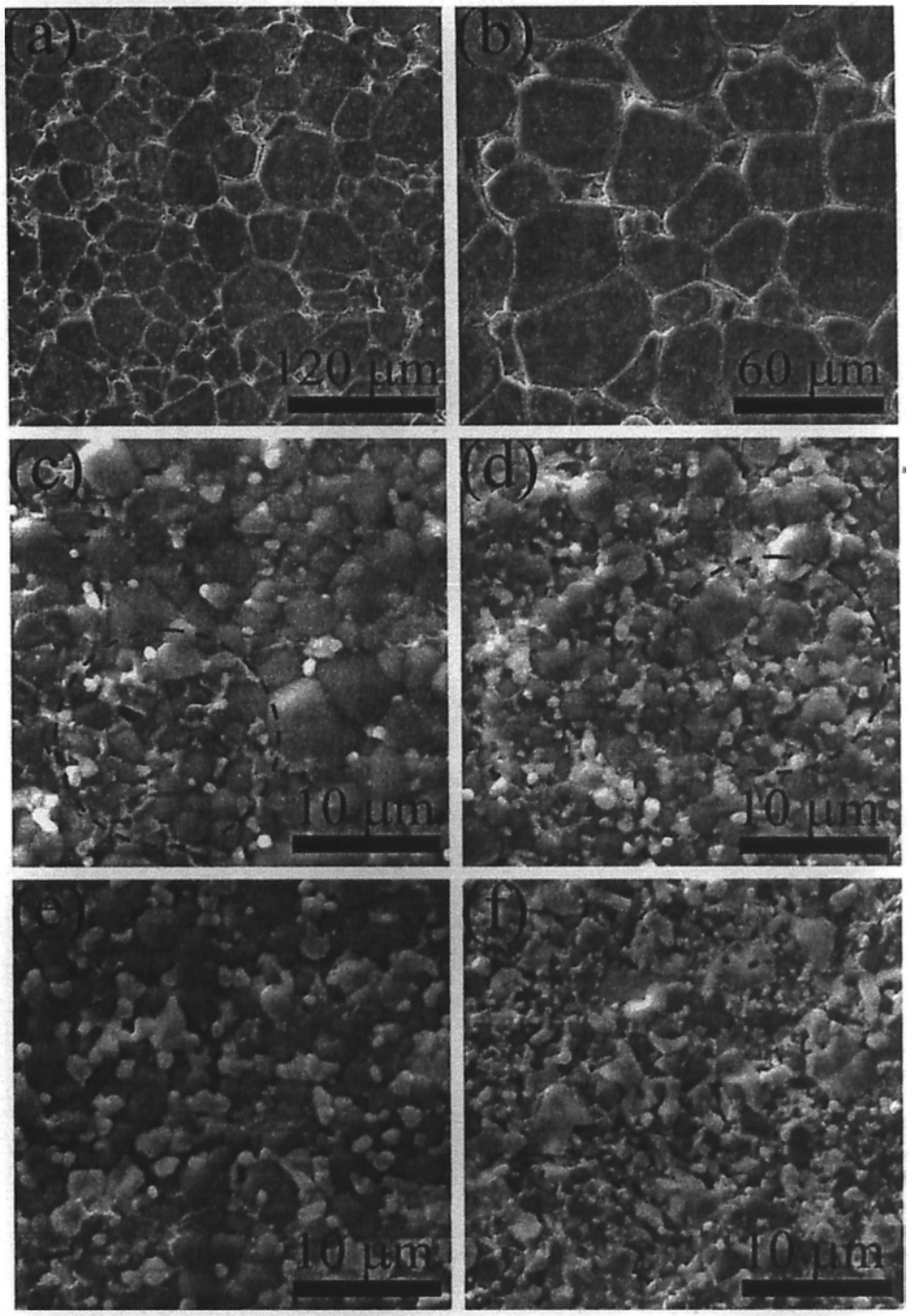

Fig. 5.6 SEM graphs of CCTO-HfO_2 ceramics for different weight ratios, (c) 20%, (d) 30%, (e) 50%, and (f) 70%. (a) and (b) with low and high magnifications correspond to the pure CCTO ceramic.

In Fig. 5.7, we present the frequency variation of the dielectric constant (ε') and loss (D) of CCTO-HfO_2 ceramics containing different HfO_2 contents. As expected, ε' decreases with increasing HfO_2 content. It is easy to see that in all the CCTO-HfO_2

ceramics, ε' is much larger than that of the pure HfO_2 sample, but smaller than that of the pure CCTO sample, which is caused by the reduction of CCTO grain size due to the addition of HfO_2. The dielectric constant and loss mainly undergo two relaxations: one in the low frequency region and the other at high frequencies. Furthermore, the low-frequency dielectric constant dispersion increases with increasing HfO_2 content in Fig. 5.7(a), which is believed to be resulted from the space charge effects at the sample surfaces, normally recognized as the electrode effects. In the present study, the sample surfaces are more insulating because of more HfO_2 content than the pure CCTO sample, hence the introduction of HfO_2 reinforces the effect of electrical polarization, leading to stronger electrode effects. In Fig. 5.7(b), we notice the low-frequency relaxation peak in D becomes stronger with increasing HfO_2, which is consistent with the observation shown in Fig. 5.7(a). Generally, adding HfO_2 leads to the enhancement of the surface resistivity, so the sample surface layer blocks more charge carriers, leading to the increase of D in the low frequency region. Afterward we proceed to the high frequency relaxation, and observe that the dielectric loss at frequencies higher than 1 kHz decreases with increasing HfO_2 content. It is noticed that the higher HfO_2 content, say greater than 20%, renders more a uniform mixing of both CCTO and HfO_2 grains, which hinders the formation of CCTO networks and cuts down the dielectric loss in the high frequency region. In addition, we observe the Debye-like relaxation peaks of dielectric loss at high frequencies shift to a lower frequency (~13 MHz) than that of the pure CCTO sample (16 MHz). We anticipate that adding HfO_2 increases the activation energy of polarization [11].

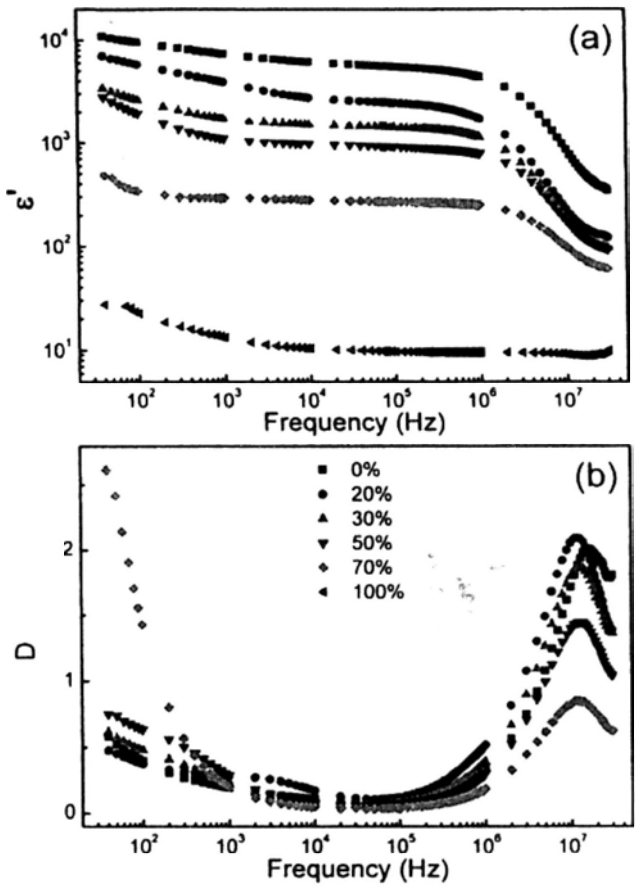

Fig. 5.7 Frequency-dependent (a) dielectric constant and (b) loss of CCTO-HfO_2 ceramics as a function of weight percent of HfO_2.

In order to clearly show the influence of adding HfO_2 on the AC conductivity (σ_{AC}), we present the dependence of σ_{AC} on the measuring frequency in Fig. 5.8. We notice that σ_{AC} increases with the frequency, and almost saturates to a constant value in the low frequency region, especially for the sample containing 70% HfO_2 as shown in Fig. 5.8(b). We can also observe that σ_{AC} decreases with an increase of HfO_2 addition in both high frequency (Fig. 5.8(a)) and low frequency regions (Fig. 5.8(b)), which implies that adding HfO_2 increases the resistivity of the samples.

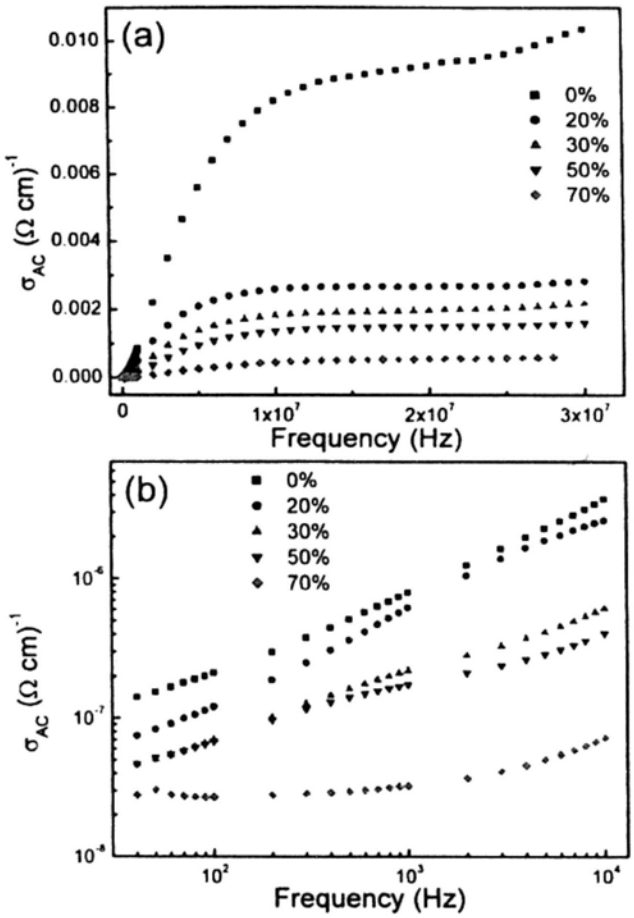

Fig. 5.8 Frequency-dependent σ_{AC} at room temperature. (b) is an enlargement part of low-frequency part of (a).

In Fig. 5.7(a), we notice that ε' values of CCTO-HfO_2 ceramics with HfO_2 weight ratios from 20% to 100% are generally smaller than that of the pure CCTO samples, yet they are much larger than that of the pure HfO_2 sample. Here we would like to present a phenomenological model to explain the large variation of the ε' values. As we learned from the previous studies, after adding a noticeable amount of HfO_2, say not less than 20%, HfO_2 aggregates between the finer and uniformly distributed CCTO grains. From Fig. 5.6, we found the CCTO grains are gradually covered up by HfO_2. Thus a "core-shell" model is constructed based on the insulating property of HfO_2 and semiconducting feature of CCTO grains, namely we regard HfO_2 as a

barrier layer enclosing CCTO grains. The same model has been successfully applied to the case of $BaTiO_3$ grains in $BaTiO_3$-CeO_2 [12], $BaTiO_3$-Nb_2O_5-Co_3O_4 [13], and $BaTiO_3$-$CdBi_2Nb_2O_9$ [14] systems, and CCTO grains in $Ca_2Cu_2Ti_4O_{12}$ (CCT-CT-1) [15] system. Most importantly, the dielectric constant values of our samples were shown to satisfy Lichtenecker's logarithmic law, which was first proposed in 1926 [16], and expressed as $ln\varepsilon'_{cal} = (1-x)ln\varepsilon'_{CCTO} + x ln\varepsilon'_{HfO_2}$, where ε'_{CCTO} and ε'_{HfO_2} represent dielectric constant values of CCTO and HfO_2 at a fixed frequency, respectively, x represents a volume fraction of HfO_2. The true density of CCTO powder was calculated by the standard method [17] using a specific gravity bottle and kerosene medium, and was found to be 4.9 g cm^{-3}. In addition, given that the density of HfO_2 as 9.68 g cm^{-3}, we can easily deduce the corresponding volume ratio values from the weight ratios. In Fig. 5.9, the calculation and experimental ε' values at 1 kHz, 10 kHz, 100 kHz, and 1 MHz are represented by a solid line and squared dots, respectively. Obviously, the experimental data are in excellent agreement with the calculated curve. Hence it provides strong support to the core-shell structure of these CCTO-HfO_2 ceramics. In addition, it is worthy to mention that the high ε' of CCTO results in the high ε' of CCTO-HfO_2 ceramics. As a result, we show a way to achieve high dielectric-constant material with other desirable properties by mixing CCTO with HfO_2.

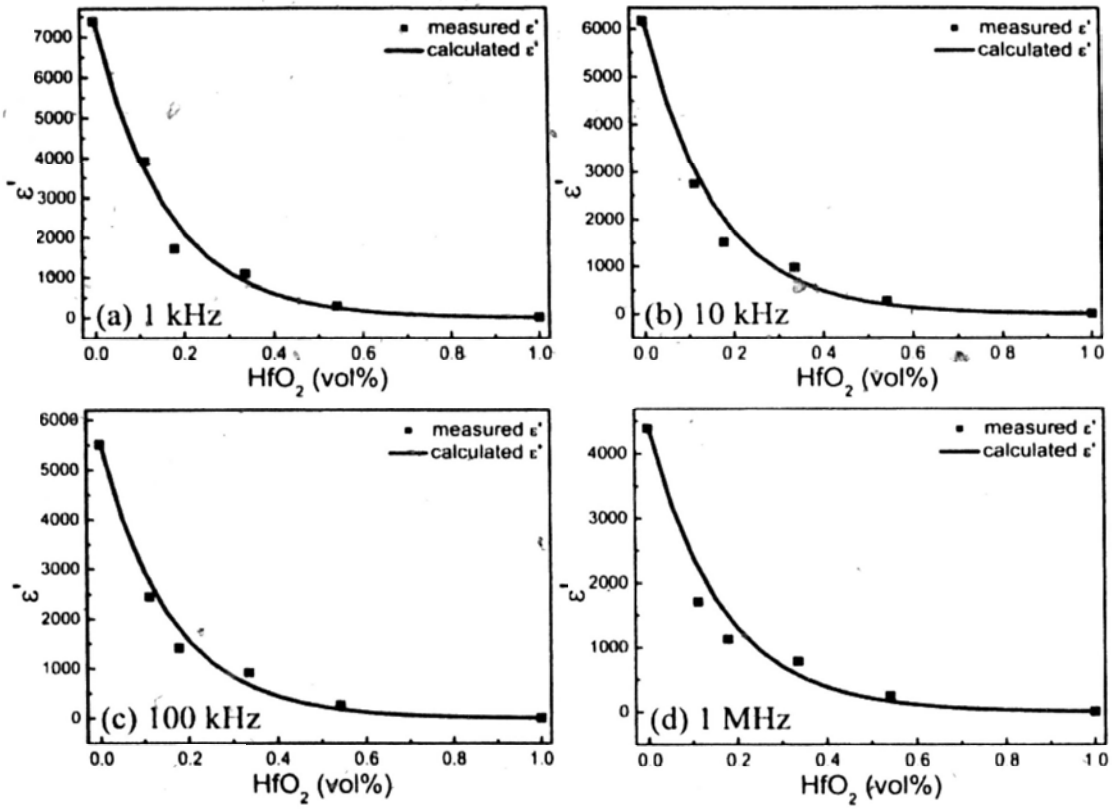

Fig. 5.9 Room temperature dielectric constant of CCTO-HfO_2 ceramics at (a) 1 kHz, (b) 10 kHz, (c) 100 kHz and (d) 1 MHz.

5.5 Conclusions

In summary, a set of CCTO-HfO_2 ceramics containing different HfO_2 weight ratios (0, 20, 30, 50, 70 and 100%) are prepared. First, their dielectric properties are measured, and both the dielectric constants and AC conductivity decrease with increasing HfO_2. It is found that the dielectric constants of CCTO-HfO_2 ceramics with high HfO_2 concentrations obey Lichtenecker's logarithmic law, which means that the distribution of CCTO grains is homogenous within the HfO_2 matrix that serves as a barrier layer.

References

[1] A.P. Ramirez, M.A. Subramanian, M. Gardel, G. Blumberg, D. Li, T. Vogt, S.M. Shapiro, *Giant dielectric constant response in a copper-titanate*, Solid State Commun. **115** (2000) 217-220.

[2] M.A. Subramanian, A.W. Sleight, *$ACu_3Ti_4O_{12}$ and $ACu_3Ru_4O_{12}$ perovskites: high dielectric constants and valence degeneracy*, Solid State Sci. **4** (2002) 347-351.

[3] T.T. Fang, H.K. Shiau, Mechanism for developing the boundary barrier layers of *$CaCu_3Ti_4O_{12}$*, J. Am. Ceram. Soc. **87** (2004) 2072-2079.

[4] P. Thomas, L.N. Sathapathy, K. Dwarakanath, K.B.Varma, Microwave synthesis and sintering characteristics of $CaCu_3Ti_4O_{12}$, Bull. Mater. Sci. 30 (2007) 567-570.

[5] M.A. Subramanian, L. Dong, N. Duan, B.A. Reisner, A.W. Sleight, *High dielectric constant in $ACu_3Ti_4O_{12}$ and $ACu_3Ti_3FeO_{12}$ phase*, J. Solid State Chem. **151** (2000) 323-325.

[6] S. Ezhilvalavan, T.Y. Tseng, *Process in the developments of $(Ba,Sr)TiO_3$ (BST) thin films for giga-bit era DRAMs*, Mater. Chem. Phys. **65** (2000) 227-248.

[7] L.C. Kretly, A.F.L. Almeida, R.S. De Olivera, J.M. Sasaki, A.S.B. Soombra, *Electrical and optical properties of $CaCu_3Ti_4O_{12}$ (CCTO) substrates for microwave devices and antennas*, *Microwave Opt. Technol. Lett.* **39** (2003) 145-150.

[8] A.F.L. Almeida, P.B.A. Fechine, J.C. Goes, M.A. Miranda, M.A.R. Miranda, A.S.B. Sombra, *Dielectric properties of $BaTiO_3$(BTO)-$CaCu_3Ti_4O_{12}$(CCTO) composite screen-printed thick films for high dielectric constant devices in the medium frequency (MF) range*, Mater. Sci. Eng. B **111** (2004) 113-123.

[9] X.Y. Zhao, D. Vanderbilt, *First-principles study of structural, vibrational, and lattice dielectric properties of hafnium oxide*, Phys. Rev. B **65** (2002) 233106.

[10] L. Marchin, A.A. Levchenko, S. Guillemet-Fritsch, A. Navrotsky, B. Durand, T. Lebey, *Grain-growth controlled giant permittivity in soft chemistry $CaCu_3Ti_4O_{12}$ ceramics*, J. Am. Ceram. Soc. **91** (2008) 485-489.

[11] F.C. Luo, J.L. He, J. Hu, Y.H. Lin, *Electric and dielectric properties of Bi-doped $CaCu_3Ti_4O_{12}$ ceramics*, J. Appl. Phys. **105** (2009) 076104.

[12] Y. Park, H.G. Kim, *The microstructure analysis of cerium-modified barium titanate having core-shell structured grains*, Ceram. Int. **23** (1997) 329-336.

[13] Y. Yuan, S. Zhang, W. You, *Preparation of $BaTiO_3$-based X7R ceramics with high dielectric constant by nanometer oxides doping method*, Mater. Lett. **58** (2004) 1959-1963.

[14] D. Hennings, G. Rosenstein, *Temperature-Stable dielectrics based on chemically inhomogeneous $BaTiO_3$*, J. Am. Ceram. Soc. **67** (1984) 249-254.

[15] W. Kobayashi, I. Terasaki, *$CaCu_3Ti_4O_{12}/CaTiO_3$ composite dielectric: Ba/Pb-free ceramics with high dielectric constants*, Appl. Phys. Lett. **87** (2005) 032902.

[16] K. Lichtenecker, *Dielectric constant of natural and synthetic mixtures*, Phys. Z. **27** (1926) 115-158.

[17] R.W. Grimshaw, *The Chemistry and Physics of clays*, London, (1971).

Chapter 6 Microstructures and dielectric properties of $CaCu_3Ti_4O_{12}$ thin films by rf magnetron sputtering method

Perovskite-like oxide $CaCu_3Ti_4O_{12}$ (CCTO) thin film attracts great interest because it has high dielectric constant and is a lead-free material. Thus it is a promising candidate for capacitor applications, microelectronics and microwave devices, where the miniaturization is crucial. In fact, CCTO thin films have been fabricated by several experimental methods, such as pulsed-laser deposition (PLD) [1-8], sol-gel [9-12], chemical solution deposition (CSD) [13-15], and metal organic chemical vapor deposition (MOCVD) [16]. In this section we report our attempts to prepare CCTO thin films using radiofrequency (rf) magnetron sputtering, which generally offers such advantages as uniform microstructure, high deposition rate, and low process temperature, and has also been proven to be a promising approach for producing thin-film capacitors in integrated circuits. Like CCTO ceramics, the dielectric properties of the thin films are found to be sensitive to the preparation process. As a result, experimental results demonstrate that the annealing temperature influences significantly the dielectric properties of the CCTO thin films. In this work, we present the effect of annealing conditions on the surface morphologies and the dielectric properties of CCTO thin films. Since our sputtered CCTO thin films are generally composed of uniform microstructures (<0.5 μm), thus they also provide a good opportunity to understand the extrinsic as well as intrinsic mechanism of low (<1 kHz) and high (> 10 MHz) frequency regions.

6.1 Experimental

The thin films were prepared on Pt/Ti/SiO_2/Si substrate using rf magnetron sputtering method as described in Chapter 1. Then the as-sputtered CCTO films were annealed for 50 min in the ambient atmosphere at various temperatures: in this work, we chose 600, 700, 800 and 900 °C. The heating rate of 20 °C/min and cooling rate of 5 °C/min. In order to rule out the influence of Ti film in the Pt/Ti/SiO_2/Si substrate during compositional analysis of the as-sputtered thin films, CCTO thin film was also deposited directly on SiO_2 substrate. For dielectric measurements, 200 nm thick Pt film served as the bottom electrode, and silver paint was used as the top electrode of the dielectric CCTO films.

The thickness of the films was measured using a Tencor Alpha-Step 500 Surface Profiler. The experimental techniques and measurement conditions used were described in Section 1.3.4.

6.2 Results and discussion

In Fig. 6.1, we present the surface morphology of the as-sputtered CCTO film on SiO_2 substrate. As we can see the film exhibits no indications of microstructural features and is smooth all over, which implies that the substrate temperature of 480 °C does not provide sufficient energy for the thin film to form grains. From the EDX analysis of the film, we deduced the atomic ratio for Ca:Cu:Ti:O to be 5.38:18.43:18.06:58.15, which implies that the film is deficient in Ti, even though the target is a stoichiometric CCTO material.

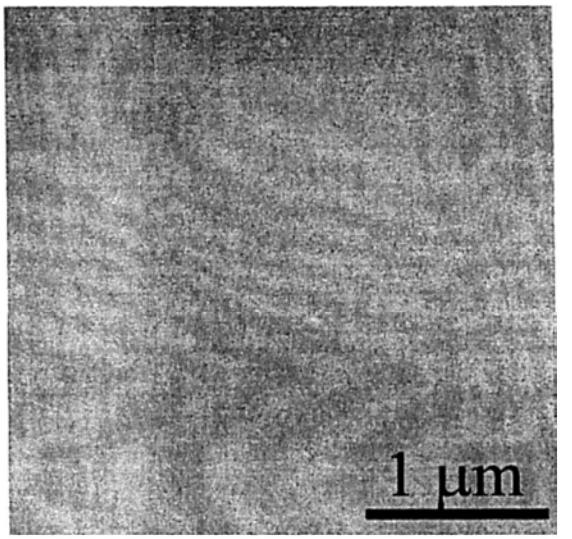

Fig. 6.1 SEM micrograph of the as-sputtered thin film on SiO_2 substrate.

In Fig. 6.2, we show the XRD patterns of the thin films annealed at different temperatures. The film annealed at 600 °C was found to be amorphous, so we did not present it. Whereas in the 700 °C sample, there are a CuO (002) peak and a weak CCTO (220) peak in the diffraction pattern. However, polycrystalline CCTO peaks clearly show up on the samples with annealing temperatures of 800 and 900 °C, in which we notice the distinct (200), (400) and (422) peaks that match with those of the CCTO phase. CuO diffraction peak also exists in the XRD graph of the 800 °C sample, but disappears from the 900 °C sample.

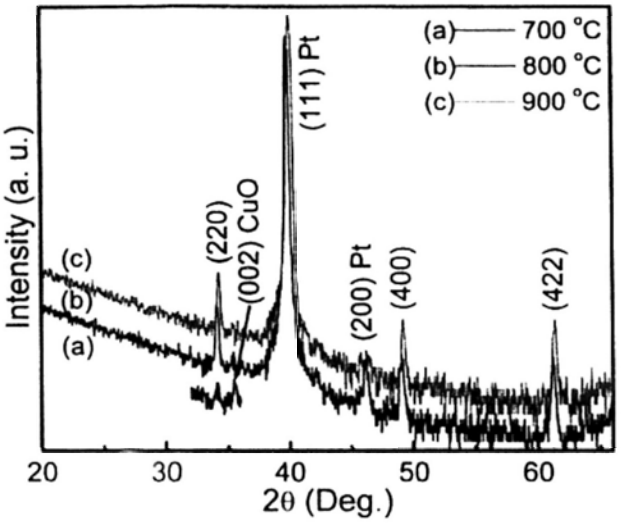

Fig. 6.2 XRD patterns for thin films annealed in air at 700, 800 and 900 °C.

In Fig. 6.3, we present the surface morphology of CCTO films that were annealed at various annealing temperatures. In the 600 °C film (Fig. 6.3(a)), there are a few grains with bright edges present on its surface. As we increased annealing temperature, the brilliant homogenous grains multiplied as shown in Figs. 6.3 (b) and (c). Yet after the film was annealed at 900 °C, most brilliant grains disappeared, and we see the background is composed of dark CCTO grains with an average size of ~0.2 μm (Fig. 6.3(d)).

We also found that the thin film thickness was not influenced by the annealing temperature, so the 900 °C sample was chosen to show the typical cross-section image of the films (Fig. 6.4), from which we deduce the film thickness as about 900 nm. This value is in good agreement with the thickness obtained from the surface profiler.

Here we adopt the EDX analysis method to find out the chemical component of the dark grains and the brilliant grains. Typical EDX spectra are obtained from the 900 °C sample, and shown in Figs. 6.5 (a) and (b), respectively. The peaks observed in

Fig. 6.5 correspond to all the known peak positions for Ca, Cu, Ti, and O elements. As we can see the Cu peaks in Fig. 6.5 (b) are much stronger than those in Fig. 6.5 (a), which implies that the brilliant grains are rich in Cu compared with the dark grains. Meanwhile, their chemical component analysis results are shown in Table 6.1. Also according to the EDX analysis combined with the XRD results shown in Fig. 6.2, the dark grains are CCTO phase, and the brilliant grains are the CuO phase.

Based on these results, we can explain the microstructures observe in Fig. 6.3. Since the as-sputtered film is Ti-deficient and relatively rich in Cu compared to the stoichiometry CCTO component, excess Cu is ejected from the films after increasing annealing temperature from 600 °C to 700 °C, which floats on the film surfaces in the form of CuO. The CCTO phase starts to form at 700 °C annealing. After annealing at 800 °C, the amount of CuO reduces. In addition, the atomic ratio of these four component elements (Ca, Ti, Cu and O) of CCTO left behind below the CuO layer is close to its stoichiometric ratio, and form a lot of CCTO phase at 800 °C. When the annealing temperature is as high as 900 °C, the CuO grains start to evaporate into air, therefore disappear from the sample surface. Therefore, this explains the changes of CuO diffraction peak in Fig. 6.2.

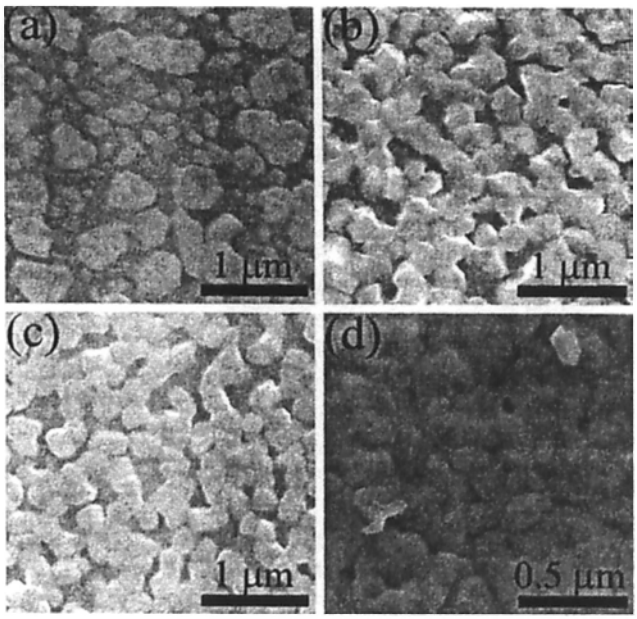

Fig. 6.3 SEM micrographs of thin films annealed in air at 600, 700, 800 and 900 °C.

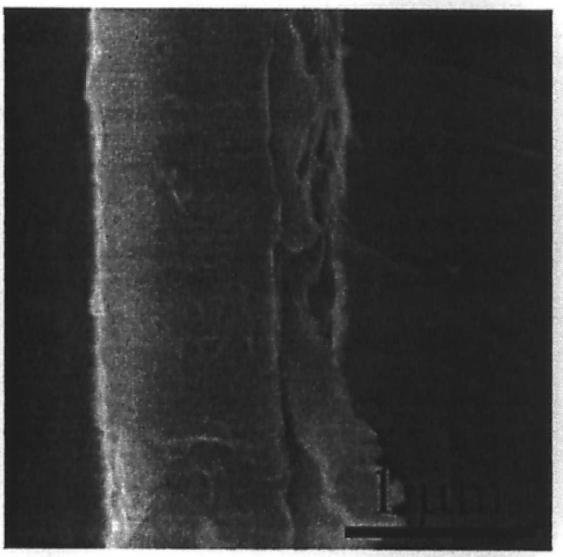

Fig. 6.4 SEM image for a cross section of the 900 °C annealed thin film.

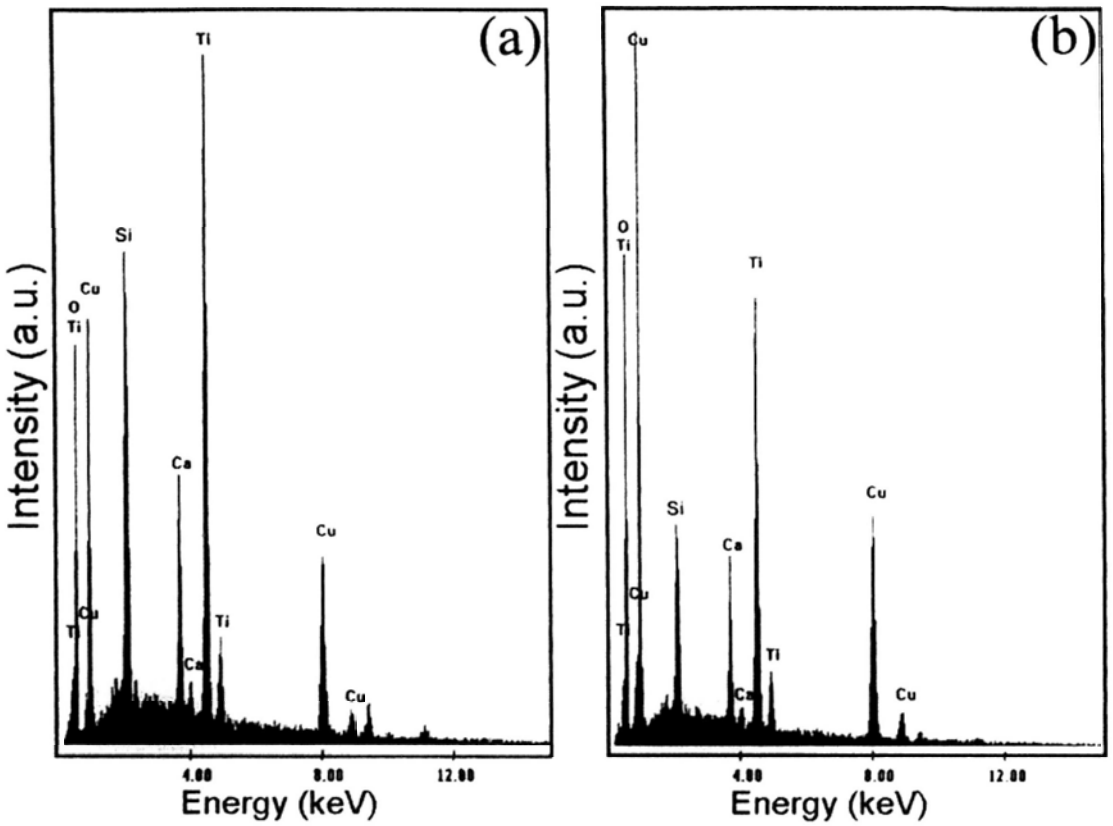

Fig. 6.5 Typical EDX images taken from (a) the dark grains and (b) the brilliant grains of the 900 °C sample.

Table 6.1 Atomic percentages (At%) of the dark and brilliant grains based on the EDX images shown in Fig. 6.5.

At%	Ca	Cu	Ti	O
dark grains	5.39	14.61	19.51	60.49
brilliant grains	4.08	19.34	13.98	62.60

In Fig. 6.6, we present the dielectric constant (ε') and loss (D) of the CCTO films annealed at various temperatures as a function of frequency. We observe that ε' decreases as frequency increases, suggesting that the temporary dipoles do not have sufficient time to follow the change of AC electric field. In the high frequency region, we notice the dramatic drop in ε' is accompanied by a corresponding peak in D. In addition, similarly to bulk CCTO ceramics, the phenomena of dielectric relaxation

can be found for all the samples. However, the relaxation frequency (10 MHz) is much higher than those (≤1 MHz) in CCTO ceramics [17] and sputtered CCTO thin films by Lin *et al.* [18]. ε' increases with annealing temperature from 700 °C to 900 °C, so we list those obtained at 1 MHz in Table 6.2. Compared with the other two samples, the one annealed at 700 °C has much smaller ε', resulting from less CCTO phase in this film. Consequently, the film annealed at 900 °C has the highest dielectric constant among the three samples. In the high frequency region (>1 MHz), the dielectric loss increases with increasing annealing temperature, which suggests that it is caused by the increased generation of oxygen vacancies during annealing.

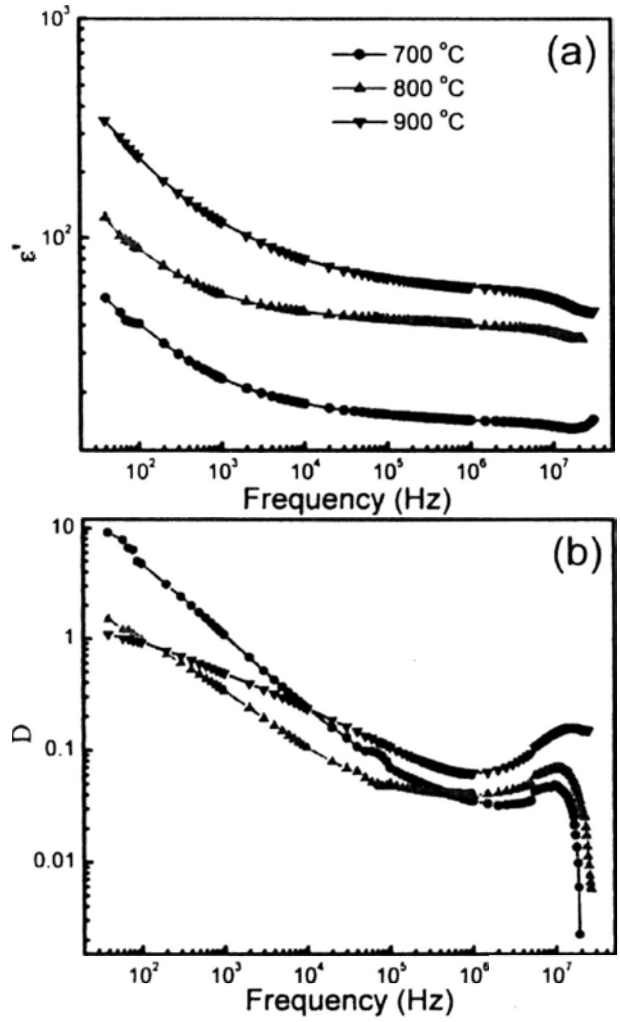

Fig. 6.6 Frequency-dependent (a) ε' and (b) D of CCTO thin films annealed at various temperatures.

Table 6.2 ε' at 1 MHz for thin films annealed at various temperatures.

T (°C)	700	800	900
ε' at 1 MHz	17.84	40.13	59.93

To further analyze the characteristic of the dielectric relaxation, we present the frequency dependence of ε' of the CCTO thin films annealed at 900 °C measured at different temperatures in Fig. 6.7. In the low temperature range (<-60 °C), there is one Debye-type dielectric relaxation, with ε'~60. With increasing temperature, we notice that the high-frequency relaxation shifts to lower frequencies, and in Fig. 6.7(b), ε' decreases from about 60 at frequencies lower than 10 MHz to an even lower value (~30) at frequency higher than 10 MHz. Then we show the change of the relaxation frequency, for convenience, using the frequency at which ε'~55 to estimate the relaxation frequency. At -195, -150, -90, -30, and 30 °C, the relaxation frequencies are 6, 4.7, 3, 2.5, and 2 MHz, respectively. This phenomenon is contrary to the characteristic of the dielectric relaxation associated with the grain-boundary IBLC model [19]. On top of that, we learned from the first principles calculation, including all the electronic and lattice contributions [20], the dielectric constant attributed to the intrinsic origin is about 40, which is very close to 60, the experimental dielectric value obtained in the high frequency region. Thus, we assert that the dielectric responses we observe in the high frequency region are mostly intrinsic. As the temperature increases to -60 °C, the dielectric constant starts to increase in the low frequency region (<1 kHz). We claim this is an indication of the presence of another Debye-type relaxation, which becomes clear at the temperatures above -30 °C. We used to attribute the origin of high ε' in the low frequency region to the extrinsic effect and associate it with the interfacial space charge polarization due to the electrode effect [21], which is caused by the charge carriers accumulating at the interface between the

electrodes and the sample surfaces. According to the report by Deng *et al.* [22,23], there is an insulating layer at the top electrode/thin film interface indicating a metal-insulator-semiconductor junction. As a result, its capacitance response, involving space charge polarization with the relaxation frequency lower than 40 Hz [24], contributes to the observed high dielectric constant in low frequency region. Furthermore, the dielectric relaxation in the low frequency region is prominent at high temperature above -30 °C, so that it is more easily to be thermally excited; hence we relate it to the polarization associated with trapped charge carrier migration at high temperature. The high temperature produces more oxygen vacancies. Therefore, more free carriers can be generated. As a result, oxygen vacancies and electrons were produced, so more charge carriers accumulate at the interface of the electrode and sample surface, leading to stronger dielectric relaxation in the low frequency region.

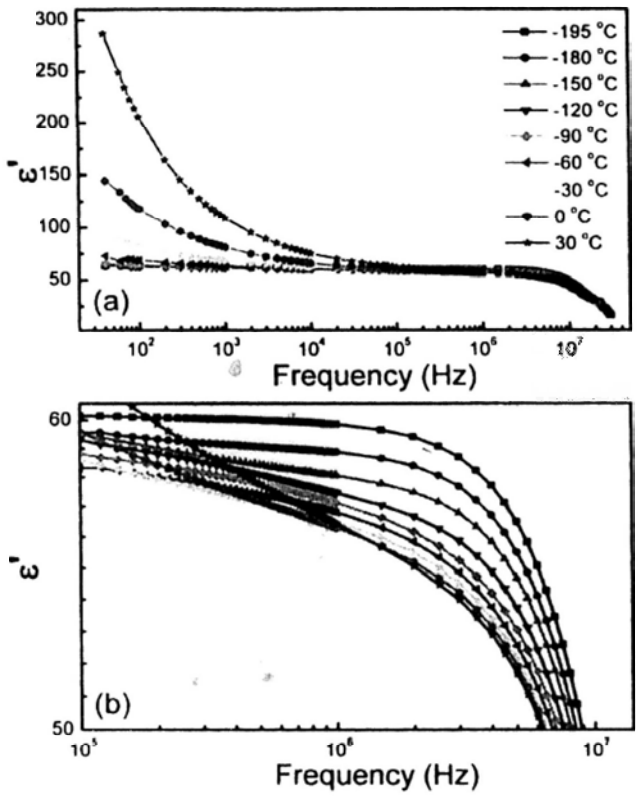

Fig. 6.7 (a) Frequency-dependent ε' of the 900 °C CCTO thin film measured at various temperatures. (b) shows the high-frequency part of (a) from 100 kHz to 10 MHz.

6.3 Conclusions

Uniform CCTO thin films with high dielectric constant were successfully synthesized by the rf magnetron sputtering method. The annealing temperature is found to influence the crystallization and microstructure of the films. As a result it also strongly affected the dielectric properties. The dielectric relaxations in low and high frequency regions were carefully investigated, and found to be extrinsic and intrinsic in origin, respectively.

References

[1] Y. Lin, Y.B. Chen, T. Garret, S.W. Liu, C.L. Chen, L. Chen, R.P. Bontchev, A. Jacobson, J.C. Jiang, E.I. Meletis, J. Horwitz, H.D. Wu, *Epitaxial growth of dielectric $CaCu_3Ti_4O_{12}$ thin films on (001) $LaAiO_3$ by pulsed laser deposition*, Appl. Phys. Lett. **81** (2002) 631-633.

[2] L. Fang, M. Shen, *Deposition and dielectric properties of $CaCu_3Ti_4O_{12}$ thin films on Pt/Ti/SiO_2/Si substrates using pulsed-laser deposition*, Thin Solid Films **440** (2003) 60-65.

[3] A. Tselev, C.M. Brooks, S.M. Anlage, H.M. Zheng, L.S. Riba, R. Ramesh, M.A. Subramanian, *Evidence for power-law frequency dependence of intrinsic dielectric response in the $CaCu_3Ti_4O_{12}$*, Phys. Rev. B **70** (2004) 144101.

[4] L. Fang, M.G. Shen, J. Yang, Z.Y. Li, *The effect of SiO2 barrier layer on the dielectric properties of $CaCu_3Ti_4O_{12}$ films*, J. Phys. D: Appl. Phys. **38** (2005) 4236-4240.

[5] L. Fang, M.G. Shen, J. Yang, Z.Y. Li, *Reduced dielectric loss and leakage current in $CaCu_3Ti_4O_{12}$/SiO_2/$CaCu_3Ti_4O_{12}$ multilayered films*, Solid State Commun. **137** (2006) 381-386.

[6] M. Mitsugi, S. Asanuma, Y. Uesu, *Origin of colossal dielectric response of $CaCu_3Ti_4O_{12}$ studies by using $CaTiO_3$/$CaCu_3Ti_4O_{12}$/$CaTiO_3$ multilayer thin films*, Appl. Phys. Lett. **90** (2007) 242904.

[7] L. Fang, M.R. Shen, *Effect of laser fluence on the microstructure and dielectric properties of pulsed laser-deposited $CaCu_3Ti_4O_{12}$ thin films*, J. Cryst. Growth **310** (2008) 3470-3473.

[8] G.C. Deng, T. Yamada, P. Muralt, *Evidence for the existence of a metal-insulator-semiconductor junction at electrode interfaces of $CaCu_3Ti_4O_{12}$ thin*

film capacitors, Appl. Phys. Lett. **91** (2007) 202903.

[9] R. Jiménez, M.L. Calzada, I. Bretos, J.C. Goes, A.S.B. Sombra, *Dielectric properties of sol–gel derived $CaCu_3Ti_4O_{12}$ thin films onto $Pt/TiO_2/Si(1\ 0\ 0)$ substrates*, J. Eur. Ceram. Soc. **27** (2007) 3829-3833.

[10] Y.W. Li, Z.G. Hu, J.L. Sun, X.J. Meng, J.H. Chu, *Preparation and properties of $CaCu_3Ti_4O_{12}$ thin film grown on LaNiO3-coated silicon by sol-gel process*, J. Cryst. Growth **310** (2008) 378-381.

[11] D.P. Singh, Y.N. Mohapatra, D.C. Agrawal, *Dielectric and leakage current properties of sol-gel derived calcium copper titanate (CCTO) thin films and CCTO/ZrO2 multilayers*, Mater. Sci. Eng. B **157** (2009) 58-65.

[12] Y.W. Li, Y.D. Shen, Z.G. Hu, F.Y. Yue, J.H. Chu, *Effect of thickness on the dielectric property and nonlinear current-voltage behavior of $CaCu_3Ti_4O_{12}$ thin films*, Phys. Lett. A **373** (2009) 2389-2392.

[13] W. Lu, L.X. Feng, G.G. Cao, Z.K. Jiao, *Preparation of $CaCu_3Ti_4O_{12}$ thin films by chemical solution deposition*, J. Mater. Sci. **39** (2004) 3523-3524.

[14] L.X. Feng, Y.W. Wang, Y.Y. Yan, G.G. Cao, Z.K. Jiao, *Growth of highly-oriented $CaCu_3Ti_4O_{12}$ thin films on $SrTiO_3$ (1 0 0) substrates by a chemical solution route*, Appl. Surf. Sci. **253** (2006) 2268-2271.

[15] V.S. Saji, H.C. Choe, *Effect of yttrium doping on the dielectric properties of $CaCu_3Ti_4O_{12}$ thin films produced by chemical solution deposition*, Thin Solid Films **517** (2009) 3896-3899.

[16] R.L. Nigro, R.G. Toro, G. Malandrino, I.L. Fragala, P. Fiorenza, and V. Raineri, *Chemical stability of $CaCu_3Ti_4O_{12}$ thin films grown by MOCVD on different substrates*, Thin Solid Films **515** (2007) 6470-6473.

[17] T.B. Adams, D.C. Sinclair, A.R. West, *Characterization of grain boundary*

impedances in fine- and coarse-grained $CaCu_3Ti_4O_{12}$ ceramics, Phys. Rev. B **73** (2006) 094124.

[18] S.Y. Lin, Y.C. Chen, C.M. Wang, K.S. Kao, C.Y. Chan, *Effect of rapid thermal annealing on sputtered $CaCu_3Ti_4O_{12}$ thin films*, J. Electro. Mater. **38** (2009) 453-459.

[19] J.J. Liu, C.G. Duan, W.G. Yin, W.N. Mei, R.W. Smith, J.R. Hardy, *Large dielectric constant and Maxwell-Wagner relaxation in $Bi_{1/2}Cu_3Ti_4O_{12}$*, Phys. Rev. B **71** (2004) 144106.

[20] L.X He, J.B. Neaton, M.H. Cohen, D. Vanderbilt, *First-principles study of the structure and lattice dielectric response of $CaCu_3Ti_4O_{12}$*, Physical Review B **65** (2002) 214112.

[21] L. Zhang, *Electrode and grain-boundary effects on the conductivity of $CaCu_3Ti_4O_{12}$*, Appl. Phys. Lett. **87** (2005) 022907.

[22] G. Deng, T. Yamada, P. Muralt, *Evidence for the existence of a metal-insulator-semiconductor junction at the electrode interfaces of $CaCu_3Ti_4O_{12}$ thin film capacitors*, Appl. Phys. Lett. **91** (2007) 202903.

[23] G. Deng, N. Xanthopoulos, P. Muralt, *Chemical nature of colossal dielectric constant of $CaCu_3Ti_4O_{12}$ thin film by pulsed laser deposition*, Appl. Phys. Lett. **92** (2008) 172909.

[24] V.V. Daniel, *Dielectric Relaxation* (New York: Academic, 1967).

Chapter 7 Conclusions

In this thesis, we focused on the syntheses, characterizations and measurements of the dielectric properties of $CaCu_3Ti_4O_{12}$ ceramics, their mixtures with three different compounds, PVA, B_2O_3, HfO_2, and CCTO thin films.

In Chapter 1, we provided a general outline of this work, starting with a brief summary of previous notable works and development of the extrinsic mechanism ideas. Then we summarized the essential schemes used to analyze the experimental data and deduce important parameters of the systems studied. Afterward, we introduced the major experimental techniques for sample preparations and characterizations.

In Chapter 2, we provided detailed studies of the CCTO ceramics using powder produced by a wet chemistry method, which has the advantages of using relatively lower temperature, 800 °C, and for shorter time, 1 h. On top of that, we noticed different sintering temperatures, such as 900 and 1050 °C, lead to high dielectric constant and different grain size: the one with the 900 °C sintering temperature has small grains ~0.3 μm, and the other has large grains, ~55 μm. More importantly, in both the samples, we found that Maxwell-Wagner relaxations of three different extrinsic origins, resulting in the high dielectric constants, were clearly separated from each other.

In the third part of the thesis, from Chapter 3 to Chapter 5, we reported findings from the studies of CCTO with different additions. Our motivation is primarily to modify the undesired dielectric loss of the pure CCTO sample; hopefully by mingling with a proper compound, we may be able to fabricate materials with a high resistivity and a reasonably high dielectric constant. In our studies, we fabricated samples by

mixing PVA, B_2O_3 and HfO_2 for their own special characteristics with CCTO at 1000 °C for 10 h using the solid state reaction method. Generally speaking, from the dielectric properties we investigated, we noticed, PVA weakens the frequency dependence of the measured dielectric constant. B_2O_3 managed to reduce the thickness of grain boundary and mitigated the non-Ohmic properties of ceramic samples. Whereas HfO_2 is an intrinsic high dielectric-constant material, it reduced the average grain size and maintained a reasonable high dielectric constant, which is smaller than the pure CCTO but greater than the pure HfO_2. Yet it rather significantly decreased the dielectric loss, which is an important parameter in the potential applications in electric devices.

Finally, in Chapter 6, we discussed the microstructure and dielectric properties of CCTO thin films prepared by rf magnetron sputtering method. We showed that when the film was annealed at 900 °C, single-phase CCTO with small grains ~0.2 μm started to form. And the dielectric relaxation frequency shifts to 10 MHz, one order higher than most reported values, <1 MHz. We attributed it mostly to the intrinsic mechanism.